NORTHERN ILLINOIS UNIVERSITY

ANALYSIS OF A PEM FUEL CELL USING A FINITE ELEMENT-BASED COMPUTATIONAL MODEL

A THESIS SUBMITTED TO THE GRADUATE SCHOOL

IN PARTIAL FULFILLMENT OF THE REQUIREMENTS

FOR THE DEGREE

MASTER OF SCIENCE

DEPARTMENT OF MECHANICAL ENGINEERING

BY

PAVAN KUMAR POTHARAJU

DEKALB, ILLINOIS

MAY 2006

ABSTRACT

Name: Pavan Kumar Potharaju **Department: Mechanical Engineering**

Title: Analysis of a PEM Fuel Cell Using a Finite Element-Based Computational Model

Major: Mechanical Engineering **Degree: Master of Science**

Approved by: **Date:**

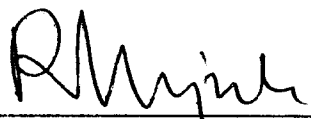

Thesis Co-Director 4/12/06

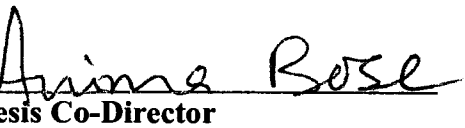

Thesis Co-Director 4/12/06

NORTHERN ILLINOIS UNIVERSITY

ABSTRACT

In recent years, fuel cells have been considered as one of the most attractive renewable energy generation systems. However, major challenges in the adaptation of fuel cell technology are to improve the performance and lower the cost of some of the critical components and materials used in fuel cells. A significant cost goes towards catalysts for PEMFC, and this requires a reduction of platinum loading on electrodes.

In order to evaluate the fuel cell system performance, a mathematical model for thermodynamics, combined heat, mass transfer processes and associated electrochemical reactions in a tri-layer PEM fuel cell design was developed to analyze the transport phenomena and reaction resistances in the micro-porous electrodes and electrolyte membranes. A finite element-based computational code was developed to solve the mathematical model and evaluate various state-of-the-art materials available in the market. The simulation model was used to conduct a sensitivity analysis to evaluate the performance of the fuel cell with varying operating conditions parameters.

Certification:

In accordance with departmental and Graduate School policies, this thesis is accepted in partial fulfillment of degree requirements.

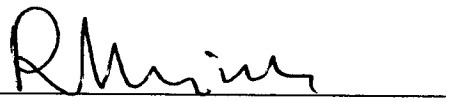

Thesis Co-Director

4/12/06

Date

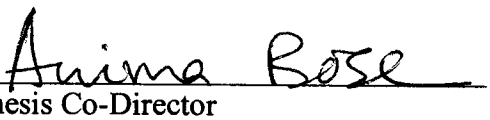

Thesis Co-Director

4/12/06

Date

TABLE OF CONTENTS

Chapter Page

LIST OF TABLES

LIST OF FIGURES

NOMENCLATURE

C	Concentration Potential	Mol/m^3
Cp	Specific Heat at constant pressure	J/Kg. K
D	Co-efficient of Diffusion	M^2/sec
E	Cell Potential	Volt
E_{rev}	Reversible Cell Potential	Volt
F	Faraday's constant (96487)	Col./mole
h	Heat-transfer Co-efficient	
i	Current Density	Amp/m^2
i_L	Limiting Current Density	Amp/m^2
i_0	Exchange current density	Amp/m^2
k	Mass-transfer Co-efficient	
K	Thermal Conductivity	W/m.K
n_e	Number of electrons	
Nu	Nusselt Number	
p	Partial Pressure	atm
P	Pressure	atm
Pr	Prandtl Number	
r_i	Electrical resistance	Ohm
R	Universal Gas Constant (8.3145)	J/mol.°K

R_e	Reynold's number	
Sc	Schmidt Number	
T	Temperature	K
U	Velocity	m/sec
x	Mole Fraction	
α	Overpotential	Volts
η	Transfer Co-efficient	
γ	Concentration Co-efficient	
ρ	Density	Kg/m^3
μ	Kinematic Viscosity	m^2/sec

CHAPTER 1

INTRODUCTION

A fuel cell is an electrochemical cell in which the energy of a reaction between a fuel, such as Hydrogen, and an oxidant, such as air/Oxygen, is converted directly and continuously into electrical energy. The research in the field of fuel cells has been increasing rapidly. The fuel cells can replace the current conventional power-generating methods, if its cost can be reduced and its performance can be improved. The fuel cells are classified into various types depending upon the electrolyte used. Among many kinds of fuel cell the polymer electrolyte membrane fuel cell (PEMFC) has gained much attention during the last 10-15 years because of its prominent features of lightweight, high-energy efficiency, high power density, non-emission and low operating temperature.

PEMFCs are seen as promising candidates for various applications ranging from small (i.e., a few watts) mobile applications up to automotive and power production applications of several kilowatts. Despite its advantages, the PEMFC is not commercialized due to its technical problems. Some of these problems are long start-up times (especially in cold climates), cell temperature control in hot climates, and lack of fuel storage techniques enabling high-energy densities. The other

hindrance to the PEMFC is due to its high cost. The cost of a fuel cell depends mainly upon the cost of the catalyst. Computational models and simulation tools can provide valuable insight and guidance for design, performance optimization, and cost reduction of fuel cells.

This thesis attempts to understand the physics and chemistry of the PEM fuel cell. A two-dimensional mathematical model is assumed to solve for the hydrogen distribution in anode, oxygen distribution in the cathode, water and temperature management in the MEA (Membrane Electrode Assembly) and the potential distribution. The mathematical model is used to perform the parametric study. This model helps in understanding the key issues like water management, thermal management, and importance of material selection for GDL and membranes. This model is used to evaluate the various losses associated within a PEMFC and helps in understanding factors affecting the overall efficiency of a PEMFC.

An isothermal, one-dimensional steady state model for PEM fuel cells was used by Springer et al. [1] in 1991. They were the first in attempting to measure the electro-osmotic drag co-efficient, water sorption isotherms, and membrane conductivities as a function of water content in the membrane by considering the water diffusion co-efficient. The advantage of thinner membrane and increase in membrane resistance with the current density was very well explained. At a given current density, the membrane resistance was observed to be decreasing with increase

in the water flux. They achieved lower membrane resistance by increasing the humidifier temperature which results in addition of water vapor content. The important conclusion of their work was that for a fully hydrated membrane, the net water per proton flux ratio was found to be as low as one-tenth of the electro-osmotic drag co-efficient, which helps in reducing the water management for PEMFC stacks.

Gottesfeld et al. [2] presented the best fit between their model and experiment for PEM fuel cell in higher current density regions over a range of cathode gas compositions. Their model explains the losses caused by interfacial kinetics; limitations of gas-transport in both catalyst layer and backing material; and ionic conductivity in the catalyst layer. Their model separated the catalyst layer attached to the membrane and catalyst layer attached to the backing layer. Their work could get the fit for not only the low and medium current density regions but also for the high current density regions. They measured the high frequency resistance PEM fuel cell in order to calculate IR losses. Polarization curves were corrected with these IR losses in order to calculate the cathode losses. They proposed that for pressurized PEFC air cathodes, the performance depended upon the electro catalysis, oxygen gas-phase transport and transport limitations in the catalyst layer. They also noticed that in humidified H2/air PEMFC, the cell limiting current depends on the gas-phase transport limitations.

Bernardi and Verbrugge [3] developed a one-dimensional mathematical model to simulate a fuel-cell electrode bonded to a polymer electrolyte membrane and investigated effect of membrane losses and polarization resistance due to oxygen

reduction reaction with varying current densities. The solution region consisted of three regions: membrane region, thin active catalyst layer, formed by the overlap of membrane gas diffusion electrode, and a gas diffusion layer. The transport model for water includes electro-potential and pressure forces. Results suggested that at high current densities, only a small portion of the active catalyst layer can be utilized and it would be more cost effective to concentrate the catalyst near the catalyst layer – gas diffusion interface.

For PEM fuel cells, Srinivasan et al. [4] derived an empirical equation using a curve-fit of the experimental data over the entire range of current densities for different temperatures, pressures, and oxygen/inert gas composition. The experimental data was obtained using PEMFC with in-house (CESHR) fabricated gas diffusion electrodes with 0.3 mg Pt/cm2 and Nafion – 115 membrane and PEMFC with E-TEK electrodes and Asahi Chemical Aciplex – S 1004 membrane. The equation showed good fit for the mass transport region and electrode kinetic parameters for Oxygen reduction.

Gurau et al. [5] developed a two-dimensional PEMFC model to solve the concentration distribution in the entire sandwich of PEM including the gas channels. Their study was a qualitative one and compared their results with the previous works. They noticed that, in case of lower values of porosity, hindrance for the cathode gas mixture to be transported towards the catalyst layer causes lower values of the limiting current density. Their model was very useful in predicting the phenomena in limiting current densities region where the effects of concentration potential are

prominent. They also observed that due to the higher inlet air velocities, the limiting current densities increase as more oxygen would be available at the catalyst layer. Unlike other models in their time, they solved the transport equations in the coupled gas channel-gas diffuser domain. They found that current density along the membrane catalyst layer interface does not show a linear distribution. They proved that temperature guides the water content, which ultimately affects the performance of the PEM fuel cell.

Ticianelli et al. [6] proposed a novel theory of impregnated Nafion® electrodes for PEM fuel cells which required just one-tenth of the catalyst used in earlier works. Cyclic voltammetry proved the active surface area to be more for these new electrodes. They noticed that the hot pressed electrodes to membrane show low activation and ohmic overpotentials. They proved that for low Nafion loading, the electrodes have poor internal electrolytic conductivity, causing poor cell performance in high current density regions. Their results depict that higher pressures and temperatures cause an improvement of the oxygen electrode kinetics and better supply of reactants at the active surface area of the electrodes. The electrode kinetic parameters at the cathode were calculated whereas at the anode mass-transportation and activation overpotentials were neglected. Their work proved that optimum humidification can enhance the fuel cell life.

Three-dimensional numerical simulations were conducted to study the integrated flow and current density distribution in two dimensions on the membrane, by Shimpalee et al. [7]. A lower and more uniform distribution of current density was

observed with the use of a diffusion layer. Their model studied the effect of membrane thickness, net water transport across the width of the flow channel, and electro-osmosis along the channel. They noticed that the concentration of Oxygen gradient needs to be more on the cathode side to diffuse towards the membrane, whereas the flow of Hydrogen is enhanced by the bulk flow towards the membrane. They asserted that in the diffusion layer not only the diffusive mechanism but also the convective transport mechanism is important and can not be neglected. Their results showed lower current densities as the diffusion layer restricts the flow of inlet gases.

Dannenberg et al. [8] proposed a two-dimensional model along the channel for PEM fuel cells. Their model helped in calculating the ohmic resistance and water profile in the MEA, current distribution, temperature distribution, and the cell performance. They employed several heat transfer co-efficient, stoichiometric amounts and various humidification temperatures to support their results. They found that the cell performance increases drastically when the humidification temperature was increased from 50 to 70 °C. This increase was explained due to the higher water content in the membrane and lower ohmic resistance at the higher humidification temperature. The cell performance was found to be increasing with the stoichiometric coefficients increasing from 0.7 to 2 and then decreasing from 2 to 3. Ohmic resistance was found to be increasing with the stoichiometric co-efficient. They noticed that for low values of heat transfer co-efficient, temperature of the fuel cell was increasing at the inlet, leading to a lowering of water content in the membrane and high ohmic resistances causing a lower current density. They showed that the best

performance of fuel cells can obtained by maintaining the operating conditions close to isothermal.

Lu et al. [9] in 2002 employed a three-dimensional, non-isothermal computational model to solve for the entire MEA and gas distribution, and flow channels without considering the phase change phenomena in PEM fuel cells. At low and medium current density regions their results correlate with the experimental data but could not support in the high current density region due to unavailability of data. Their results helped in understanding the mole fraction distribution in the cathode region which could not be known by experimentation. Temperature distribution, the major factor affecting all the transport phenomena, was precisely calculated and figured out that magnitude of temperature increases due to irreversibility. Their work clearly explained the three important processes of water transport; electro-osmosis; back diffusion; and convection for pressure gradient case.

Berning and Djilali [10] conducted a parametric study of transport phenomena in PEM fuel cells to learn the role of contact resistance on the performance of fuel cells. Their study also concentrated on the effects of temperature, pressure, and geometrical and material parameters. They stated that increase in temperature speeds up the reaction kinetics, causing an increase in the exchange current density. It was also found that the pressure affects the inlet gas composition, exchange current density, reference potential and gas-pair diffusivities. Increase in both stoichiometric flow ratio and porosity caused even distribution of local current density. The effect of operational parameters and kinetic properties on the fuel cell performance was

strongly emphasized. They concluded that precise estimation of contact resistance was required to understand the impact of porosity and channel width on cell performance.

Zhiwen et al. [11] solved a thermo-fluid model to analyze the cooling effect of the inlet gas flow rates to encounter the thermal management problem aroused due to high local temperatures in a molten carbonate fuel cell. They used the finite volume method to solve the problem and assumed 80% for Hydrogen and 20% for Oxygen utilization factors, respectively. They studied various factors affecting the performance of a fuel such as gas utilization factor, cell temperature distribution, species distribution, etc. They found that at low current density region, thermal energy converted from the activation overpotential, and concentration overpotential increased the cell temperature. It was also observed that at the high current density region, concentration overpotential would be high as more fuel would be consumed. The cooling effect of the inlet gases proved to increase the life of the cell, particularly for high power generating applications.

Song et al. [12] attempted to numerically optimize the parameters for the catalyst layer of PEM fuel cells. Their model optimized parameters like Nafion content, platinum loading, catalyst layer thickness and porosity to achieve optimum current densities at the catalyst layer. Among these parameters, thickness was stated to be the most sensitive parameter. Their results showed that by considering the two-parameter optimization on thickness and Platinum loading of the catalyst layer, best performance could be obtained. They concluded that optimization accuracy could be

increased by studying characteristics like the relation between the effective and the bulk diffusion co-efficient, Oxygen diffusion in a combination of Nafion and Liquid water.

The objective of this thesis is to develop a finite element-based computational model to simulate the distribution of gases in the tri-layer PEMFC by solving the model using continuum mechanics. The mathematical model involves transport equations of gas and ion concentrations, water, temperature and potential distributions in the tri-layer and transport equations for gas flow in anode and cathode channels. A solution algorithm integrating the thermodynamics of electro-chemical reactions and solution transport equations will be developed and implemented into a computer code. The model was validated by comparing results with those available in the literature. The performance in terms of effective distribution gases, current densities, water distribution and polarization will be analyzed. A parametric study will be conducted to evaluate the performance with varying operating parameters and conditions.

CHAPTER 2

MATHEMATICAL MODELING

This chapter presents the thermodynamic model for electrochemical reactions and transport models for species, heat, water and electrical potential in a tri-layer PEM fuel cell. A solution algorithm is also presented to simulate the performance characteristics of the PEM fuel cell.

Physical Model of Tri-layer PEM Fuel Cell

A fuel cell system consists of an electrolyte media sandwiched between two electrodes: Anode and Cathode as shown in Fig. 2.1.

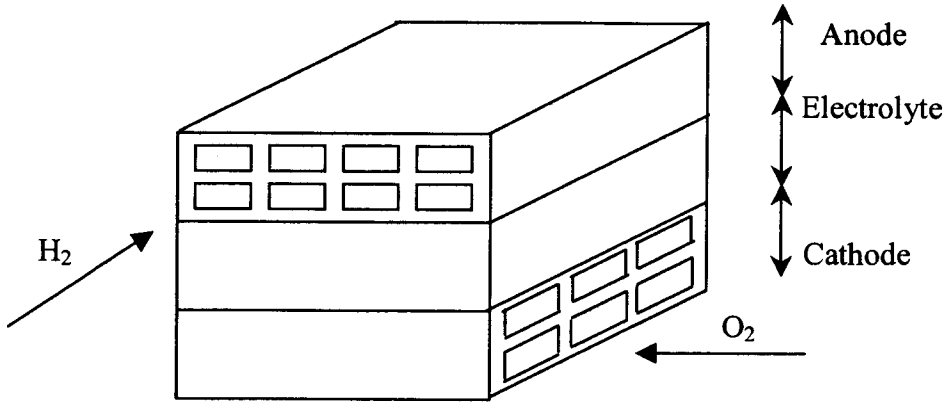

Figure 2.1. Schematic of a PEM Fuel Cell.

Humidified H_2 enters the anode gas channels and humidified Oxygen/air enters the cathode gas channels. Hydrogen diffuses through the gas the diffusion layer towards the catalyst coated anode electrode-electrolyte interface where two electrons and two protons (H^+) are formed per mole of H_2. Electrons released from the hydrogen at the anode pass through the conductive diffusion layer toward and external circuit (Load) to the cathode electrode. The H^+ migrates through the electrolyte media towards the cathode. At the catalyst coated cathode-electrolyte interface, the electron and H^+ combines with Oxygen gas supplied to form water. Heat is generated during this reaction, as it as an exothermic reaction. The purpose of the electrolyte is to transport the protons towards the cathodes and to conduct the ionic charge between the anode and cathode electrodes. The details of anodic and cathodic reactions along with the type of mobile ions depend on the fuel cell types made with different electrolytes. A Platinum catalyst is required in both anodic and cathodic reactions for low temperature electrochemical reactions. A Proton Exchange Membrane (PEM) uses polymers as carrier of ions.

Electrochemical Reactions

The fuel cell produces energy from the electrochemical reactions. Both the anodic and cathodic reactions require a precious catalyst to perform the reaction in a PEMFC. To calculate the energy generated from the electrochemical reactions, it is very important to consider both the half cell reactions separately. The algebraic sum of half cell potentials gives the output voltage. The catalyst (mostly Pt) does not take

part in the reaction; it provides activation energy to increase the rate of reaction. The half cell reactions and the total reaction are shown below.

Anode Reaction $H_2 \rightarrow 2H^+ + 2e^-$ ... (2.1)

Cathode Reaction $\frac{1}{2}O_2 + 2e^- \rightarrow O^{2-}$ ... (2.2)

Overall Reaction $2H^+ + O^{2-} \rightarrow H_2O$ ... (2.3)

Electrode Material and Structure

Reactions at the electrode are surface phenomena, and require large exposed effective surface area to sustain continuous reactions. In order to achieve a large surface area, the electrodes are made in the form of porous structures. The pore structure may be in the form of a micro-porous carbon cloth or paper through which reactant gas diffuses towards the interface. The electrodes are characterized by the thickness and pore structure. The rate of reaction depends upon the amount of active surface area available. An active surface area is a region where the reactant gas has access to electrode material, electrolyte and catalyst particles.

Catalyst Layer

A catalyst layer is added in order to enhance the electrochemical reaction and to reduce activation overpotential. The catalyst layer can be sprayed in a thin layer on the electrode. Another attractive way of forming the catalyst layer is to form the portion of the electrode as a porous carbon impregnated pore structure coated with platinum catalyst particles. The catalyst in real life is a very complex phenomenon. The catalyst is characterized by the surface area of the catalyst by mass of carbon support. The active surface area is the region where electrode, electrolyte, catalyst is present. It was observed that reactions takes place at these regions.

In this work, catalyst layer and electrode material are considered to be distinct layers in order to simplify the actual complex structure for the analytical solution. Mathematically, the catalyst layers in PEM fuel cells can be classified into three types.

The catalyst is brushed or sprayed onto the electrodes. The catalyst coating can be mathematically represented as shown in Fig. 2.2 shows the thin layer of catalyst sandwiched between the electrode and membrane.

Another type of classification is where the catalyst layer would exist and some part of the catalyst is assumed to be protruded inside the electrode material to increase the active surface area as shown in Fig. 2.3

The other type of catalyst is where the catalyst layer is assumed to be impregnated inside the membrane as shown in Fig. 2.4. Even this type is used to increase the active surface area.

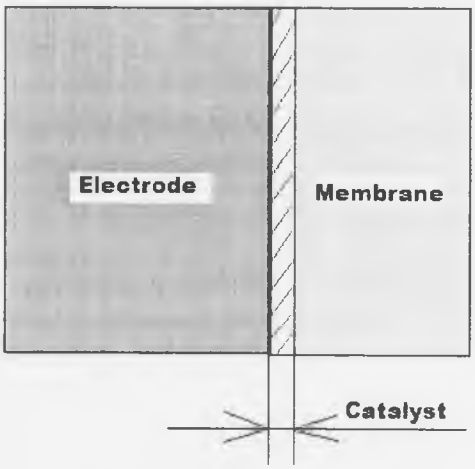

Figure 2.2. Catalyst with monolayer.

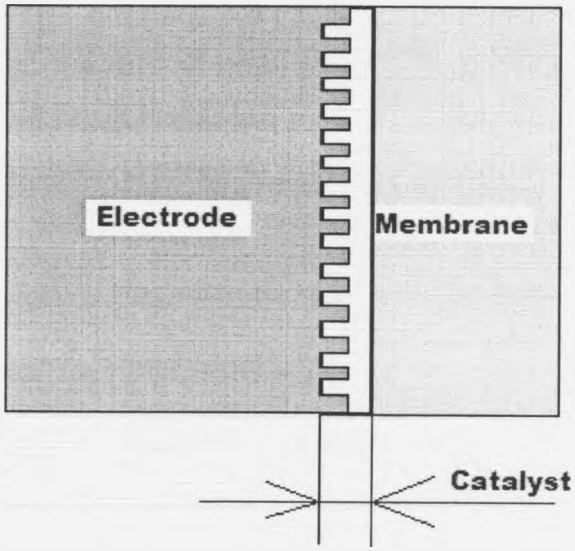

Figure 2.3. Catalyst monolayer protruded into electrode.

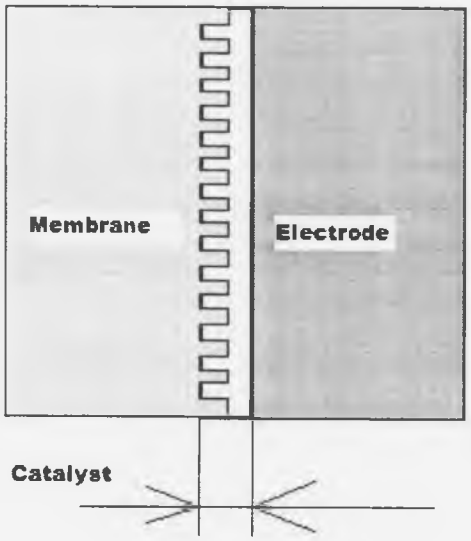

Figure 2.4. Catalyst monolayer protruded into membrane.

Electrolyte Membrane

The purpose of the polymer electrolyte is to transport the proton or H^+ from anode to cathode side. Since proton conductivity depends on water concentration in the membrane, it is essential that the membrane is sufficiently hydrated in order to sustain an effective transport of the ion, and thus maintain the reaction at the desired level. The polymer membrane such as Nafion is designed to include a large amount of hydrophilic regions through which proton or H^+ ions can migrate efficiently.

Gas Flow Channels

The gas diffusion layers are designed for effective transport of gas species through the GDL to get homogeneous distribution at the catalyst layer. The flow field as well as the energy and mass transport in the gas channels play a significant role in the distribution gas species and hence in the current density at the electrode-electrolyte interface.

Thermodynamic Model

Electro-chemical reactions are given as

Reaction at anode:

Hydrogen molecules supplied at the anode electrode ionizes releasing electrons (e^-) and forming two H^+ from each molecule. The reaction is written as

$$H_2 \rightarrow 2H^+ + 2e^- + \Delta G_1 \quad \ldots (2.4)$$

Reaction at cathode:

Each oxygen molecule reacts with two electrons and a H^+ to form water.

$$\frac{1}{2}O_2 + 2e^- + 2H^+ \rightarrow 2H_2O + \Delta G_2 \quad \ldots (2.5)$$

Overall reactions:

$$H_2 + \frac{1}{2}O_2 \rightarrow H_2O + \Delta G \quad \ldots (2.6)$$

Where

$$\Delta\overline{G} = \Delta\overline{G}_1 + \Delta\overline{G}_2 = \text{Total Gibbs' free energy} \quad \ldots (2.6)$$

The Gibbs's free energy of formation released in a electrochemical reaction depends on associated temperature and pressure and is given by the difference of the Gibbs free energy of formation of the products and the reactants given as

$$\Delta\overline{G} = \Delta\overline{G}_{H_2O} - \Delta\overline{G}_{H_2} - \Delta\overline{G}_{O_2} \quad \ldots (2.7)$$

For an ideal or reversible system the total Gibb's free energy is transformed into electrical work done.

$$\Delta\overline{G} = -nFE \quad \ldots (2.8)$$

Where n = no. of electrons in reaction per mole;

E = cell voltage or electromotive force; and

F = Faraday's constant = 96487 Col.

So, in a reaction that transfers n electrons for each molecule of fuel the reversible potential is given as

$$E_{rev} = -\frac{\Delta\overline{G}}{nF} \quad \ldots (2.9)$$

And the total Gibb's energy expressed so far is the thermodynamic Gibb's energy obtained ideally in equilibrium reaction. The real energy is expressed net Gibss energy as

$$\Delta\overline{G}_{net} = \Delta\overline{G}_{thermo} - \Delta\overline{G}_{masstransfer} - \Delta\overline{G}_{kinetics} \quad \ldots (2.10)$$

Nernst Equation-Effect of Temperature and Pressure on Gibbs Function

The change in Gibbs' function is usually in terms of the activity co-efficient. For reactions involving gas mixture the activity co-efficients can be replaced by the partial pressures. The change in Gibbs function is given as

$$\Delta G = \Delta G^0 + RT \ln \frac{P_M^{n_M} P_N^{n_N}}{P_A^{n_A} P_B^{n_B}} \qquad \ldots (2.11)$$

where the P_M and P_N are the partial pressure of the components M and N in the products, and P_A, P_B are the partial pressure of the reactant component. For the electro-chemical reaction with direct hydrogen and oxygen, we can write the expression for the change in Gibbs energy as,

$$\Delta G = \Delta G^0 + RT \ln \frac{P_{H_2O}^n}{P_{H_2}^{n_{H_2}} P_{O_2}^{n_{O_2}}} \qquad \ldots (2.12)$$

$$\Delta G = \Delta G^0 + RT \ln \frac{P_{H_2O}}{P_{H_2} P_{O_2}^{1/2}} \qquad \ldots (2.13)$$

Combining equations Eq. (2.12) and Eq. (2.13) we get the Nernst equation for the cell reversible potential as

$$E_{rev} = \Delta G^0 - RT \ln \frac{P_{H_2O}}{P_{H_2} P_{O_2}^{1/2}} \qquad \ldots (2.14)$$

where

ΔG^0 is the standard Gibbs free energy change of the reaction

E^0 = is standard reversible electrode potential

$$= -\frac{\Delta G^0}{nF} \qquad \ldots (2.15)$$

Butler-Volmer Equation – Local Current Density

Butler-Volmer equation gives the relation between space co-ordinates and local current density distribution. Depending upon the distribution of H_2 gas distribution in Anode and O_2 gas distribution in Cathode the local current density is calculated as

Cathode local current density:

$$i_c = i_{o,c}^{ref}\left(\frac{C_{O_2}}{C_{O_2}^{ref}}\right)^{\gamma_{O_2}}\left[\exp\left(\frac{\alpha_a F}{RT}\eta_{act,c}\right)-\exp\left(-\frac{\alpha_a F}{RT}\eta_{act,c}\right)\right] \quad \ldots(2.16)$$

Anode local current density:

$$i_a = i_{o,a}^{ref}\left(\frac{C_{H_2}}{C_{H_2}^{ref}}\right)^{\gamma_{H_2}}\left[\exp\left(\frac{\alpha_a F}{RT}\eta_{act,a}\right)-\exp\left(-\frac{\alpha_a F}{RT}\eta_{act,a}\right)\right] \quad \ldots(2.17)$$

where,

$i_{o,c}^{ref}$ = Cathode reference current density

$i_{o,a}^{ref}$ = Anode reference current density

$C_{H_2}^{ref}$ = Reference Hydrogen Concentration

$C_{O_2}^{ref}$ = Reference Oxygen Concentration

γ_{H_2} = Hydrogen Concentration parameter

γ_{O_2} = Oxygen Concentration parameter

Heat and Mass Transport Model

A mathematical model for combined heat and mass transfer process in MEA is developed for the fuel cell. Electro-chemical reactions and thermodynamic equations are solved to get the boundary conditions for calculating the efficiency of fuel cell.

The transport equations for species and energy in porous electrodes, electrolyte membrane, and reactant gas flows in gas channels are derived based on conservation of species and energy over a differential element, shown in Fig 2.5 as follows.

Mathematical Description:

Let Z_1=Ach

$Z_2=A_{ch}+A_{GDL}+A_c$

$Z_3= A_{ch}+A_{GDL}+A_c+M_L$

$Z_4= A_{ch}+A_{GDL}+A_c+M_L+C_c+C_{GDL}$

$Z_5= A_{ch}+A_{GDL}+A_c+M_L+C_c+C_{GDL}+C_{ch}$

X_1=H

Here,

A_{ch} – Width of Anode gas channel

A_e – Width of Anode gas diffusion layer

M_L – Width of Membrane

C_e – Width of Cathode gas diffusion layer

C_{ch} – Width of Cathode gas channel

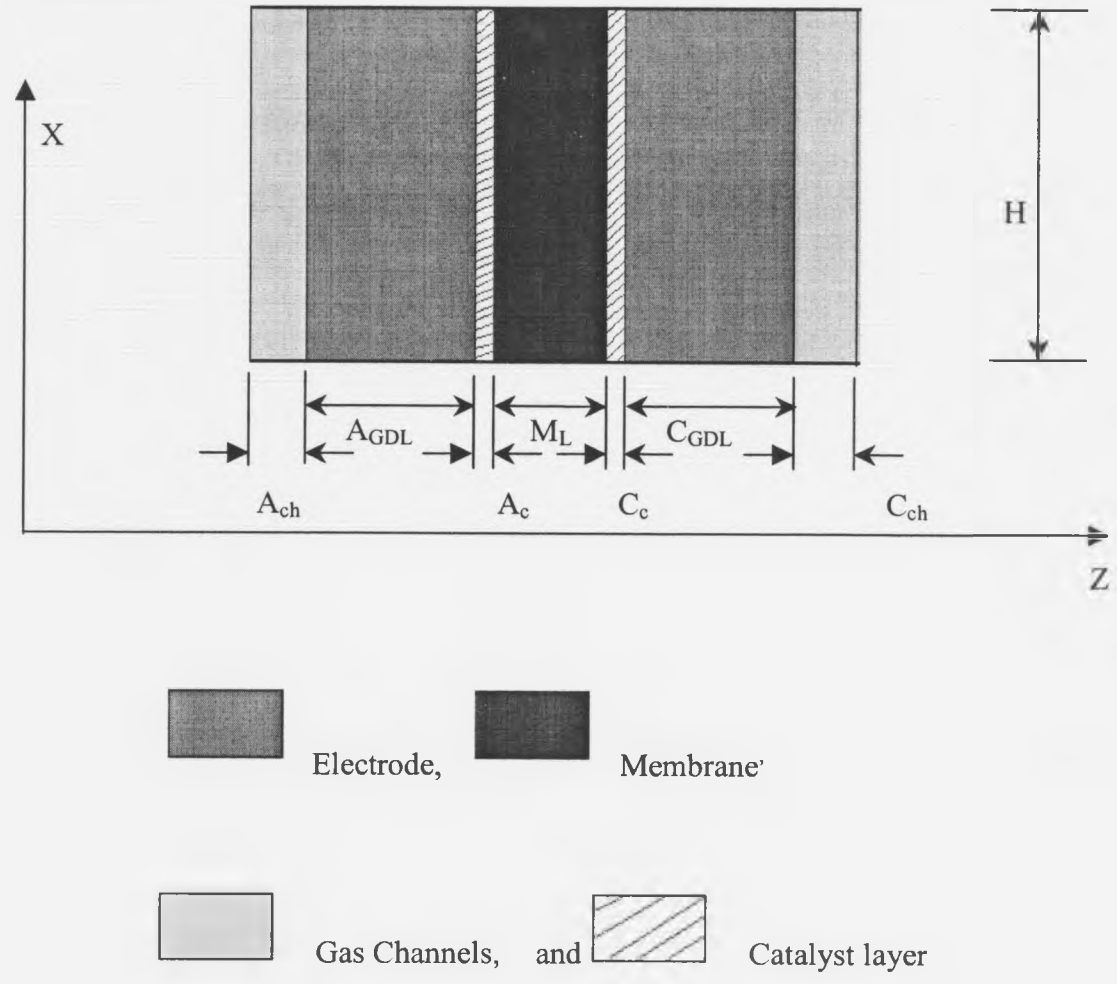

Figure 2.5. Mathematical domain for PEM fuel cell.

Transport Model

List of basic assumptions:

- Steady State
- Two-dimensional
- Constant inlet velocity
- Gases considered are ideal gases
- The membrane considered is fully hydrated so that the electronic conductivity is constant
- Hydrogen cross-over is neglected
- The catalyst layer considered is mono layer to incorporate the sink and source terms.
- Both water phase and gas phase are considered to be distinct in the diffusion layer.
- Temperature and Diffusivity are distinct.
- Flow of gases and ions are considered distinctly.

Algorithm

The equations used in the above flow chart are explained in this section. The input data is mentioned in a separate file. Initially, all the input is read into the program at once. Then the series of equations are solved as explained below.

For calculating the partial pressures exerted in the anode and cathode gas channel

$$p_{ji} = xJ(i) * P_j \quad \ldots (2.18)$$

where

p_{ji} = partial pressure exerted by the gas component 'i'

$xJ(i)$ = mole fraction of the gas component 'i'

P_j = Total pressure at the inlet

i = (H_2+ water) or (O_2+ water)

j = Anode or Cathode

The effective values of molecular weight, thermal conductivity, kinematic viscosity and specific heat at constant pressure are calculated by multiplying the corresponding quantities with the mole fraction.

The inlet velocities in channels are calculated for different species. The equation which guides the velocity is:

$$U_{inA} = \left(\frac{Stoic * i}{neA * F}\right) * \left(\frac{ny * dxx}{AaCh}\right) * \frac{R_{mixA} * T_a}{xA1 * P_a} \quad \ldots (2.19)$$

Stoic = Stoichiometric constant

I = current density

dxx = incremental distance in 'X' direction

nx = number of divisions in 'X' direction

AaCh = width of gas channel in 'Z' direction

The density, Reynolds's number, Prandtl number and Schimdt number are calculated based on the effective values.

$$\rho_A = \frac{P_A}{R_{mixA} * T_A} \quad \ldots (2.20)$$

where

ρ_A=Density of gas mixture in gas channel

PA = Pressure at inlet

RmixA = Gas constant of the gas mixture

Ta = Temperature at the inlet

$$\mathrm{Re}_A = \frac{\rho_A * U_{inA} * AaCh}{\mu_A} \quad \ldots (2.21)$$

Re_A = Reynold's number

μ_A = kinematic viscosity

$$\mathrm{Pr}_A = \frac{\mu_A * Cp_A}{K_A} \quad \ldots (2.22)$$

Pr = Prandtl number

CpA = Specific heat at constant pressure

$$Sc_A = \frac{\mu_A}{\rho_A * D_a} \quad \ldots (2.23)$$

where

Sc_A = Schmidt number

D_a = Diffusion co-efficient

The sink and source terms were calculated as

$$Sink_{H_2} = -\frac{\mu_{H_2 i} * i * dxx}{2 * F} \quad \ldots (2.24)$$

$$Sink_{O_2} = -\frac{\mu_{O_2 i} * i * dxx}{4 * F} \quad \ldots (2.25)$$

$$Source_{H_2O} = \frac{\mu_{H_2O} * i * dxx}{4 * F} \quad \ldots (2.26)$$

$$Source_{Heat} = \left(\left(\frac{Ta * \Delta s}{2 * F}\right) + \eta_{act}\right) * i \quad \ldots (2.27)$$

The Sherwood number would be calculated based on the Reynold's number and Schmidt number.

$$Sh = 3.66 + \left(\frac{0.0668 * \left(\frac{AaCh * \mathrm{Re}_A * Sc_A}{i}\right)}{1 + \left(\frac{0.04 * AaCh * \mathrm{Re}_A * Sc_A}{i}\right)^{2/3}}\right) \quad \ldots (2.28)$$

$$Nu_x = 3.66 + \left(\frac{0.0668 * \left(\frac{AaCh * \mathrm{Re}_A * \mathrm{Pr}_A}{i}\right)}{1 + \left(\frac{0.04 * AaCh * \mathrm{Re}_A * \mathrm{Pr}_A}{i}\right)^{2/3}}\right) \quad \ldots (2.29)$$

The mass transfer co-efficient and heat transfer co-efficient is calculated as

$$k_x = \frac{Sh_A * D_A}{i} \quad \ldots (2.30)$$

$$h_x = \frac{Nu_x * K_A}{i} \quad \ldots (2.31)$$

The overpotential are then calculated.

Activation overpotential:

$$\eta_{act} = b \ln\left(\frac{i}{i_0}\right) \quad \ldots (2.32)$$

Ohmic overpotential:

$$\eta_{ohm} = i^2 . r_i \quad \ldots (2.33)$$

Concentration over potential:

$$\eta_{conc} = \frac{RT}{nF} \ln\left(1 - \frac{i}{i_L}\right) \quad \ldots (2.34)$$

The terminal cell potential is calculated by the following formula.

$$E = E_{0,rev} - \eta_{act} - \eta_{ohm} - \eta_{protonic} - \eta_{concentration} \quad \ldots (2.35)$$

Governing Equations

In Anode Gas Diffusion Layer:

$$-\left(\frac{\partial}{\partial z}\left(D_i \frac{\partial C_i}{\partial z}\right) + \frac{\partial}{\partial x}\left(D_i \frac{\partial C_i}{\partial x}\right)\right) = 0 \quad \ldots (2.36a)$$

$$-\left(\frac{\partial}{\partial z}\left(K_i \frac{\partial T_i}{\partial z}\right)+\frac{\partial}{\partial x}\left(K_i \frac{\partial T_i}{\partial x}\right)\right)=0 \qquad \ldots (2.36b)$$

where i=H_2, water

In Cathode Gas Diffusion Layer:

$$-\left(\frac{\partial}{\partial z}\left(D_i \frac{\partial C_i}{\partial z}\right)+\frac{\partial}{\partial x}\left(D_i \frac{\partial C_i}{\partial x}\right)\right)=0 \qquad \ldots (2.37a)$$

$$-\left(\frac{\partial}{\partial z}\left(K_i \frac{\partial T_i}{\partial z}\right)+\frac{\partial}{\partial x}\left(K_i \frac{\partial T_i}{\partial x}\right)\right)=0 \qquad \ldots (2.37b)$$

where i=O_2, water

In Membrane:

$$-\left(\frac{\partial}{\partial z}\left(D_m \frac{\partial C_{H_2O}}{\partial z}\right)+\frac{\partial}{\partial x}\left(D_m \frac{\partial C_{H_2O}}{\partial x}\right)\right)=0 \qquad \ldots (2.38a)$$

$$-\left(\frac{\partial}{\partial z}\left(K_m \frac{\partial T_{H_2O}}{\partial z}\right)+\frac{\partial}{\partial x}\left(K_m \frac{\partial T_{H_2O}}{\partial x}\right)\right)=0 \qquad \ldots (2.38b)$$

where m=H_2O

In Anode Gas Channel:

$$u_i \frac{\partial C_{i\infty}}{\partial x} = K_{yi}(C_{\infty i} - C_i) \qquad \ldots (2.39a)$$

$$u_i \frac{\partial T_{i\infty}}{\partial x} = h_{yi}(T_{\infty i} - T_i) \qquad \ldots (2.39b)$$

where i = H_2, water

In Cathode Gas Channel:

$$u_i \frac{\partial C_{i\infty}}{\partial x} = K_{yi}(C_{i\infty} - C_i) \quad \ldots (2.40a)$$

$$u_i \frac{\partial T_{i\infty}}{\partial x} = h_{yi}(T_{i\infty} - T_i) \quad \ldots (2.40b)$$

where i=O_2, water

Boundary Conditions for Mass Transfer Equations:

At Anode GDL:

at z=Z_1 $$-D_a \frac{\partial C_i}{\partial z} = K_a(C_\infty - C_i) \quad \ldots (2.41a)$$

at z=Z_2 $$-D_a \frac{\partial C_i}{\partial z} = m''_{sa} \quad \ldots (2.41b)$$

at x=0 $$-D_a \frac{\partial C_i}{\partial x} = 0 \quad \ldots (2.41c)$$

at x=X_1 $$-D_a \frac{\partial C_i}{\partial x} = 0 \quad \ldots (2.41d)$$

where i=H_2, water

At Cathode GDL:

at z=Z_3 $$-D_c \frac{\partial C_i}{\partial z} = m''_{sc}$$ ... (2.42a)

at x=Z_4 $$-D_c \frac{\partial C_i}{\partial z} = K_c (C_\infty - C_i)$$ ... (2.42b)

at x=0 $$-D_c \frac{\partial C_i}{\partial x} = 0$$ ... (2.42c)

at x=X_1 $$-D_c \frac{\partial C_i}{\partial x} = 0$$ ... (2.42d)

where i=O_2, water

<u>At Membrane:</u>

at z=Z_2 $$-D_m \frac{\partial C_m}{\partial z} = m''_{sa}$$ ... (2.43a)

at z=Z_3 $$-D_m \frac{\partial C_m}{\partial z} = m''_{sc}$$ ... (2.43b)

at x=0 $$-D_m \frac{\partial C_m}{\partial x} = 0$$ ... (2.43c)

at x=X_1 $$-D_m \frac{\partial C_m}{\partial x} = 0$$ ... (2.43d)

Boundary conditions for Heat Transfer Equations

<u>In Anode GDL:</u>

at z=ach $$-K_a \frac{\partial T_i}{\partial z} = h_a (T_\infty - T_i)$$ ... (2.44a)

at z=agdl $$-K_a \frac{\partial T_i}{\partial z} = -K_m \frac{\partial T_i}{\partial z}$$ ... (2.44b)

at x=0 $$-K_a \frac{\partial T_i}{\partial x} = 0$$ ... (2.44c)

at x=L $$-K_a \frac{\partial T_i}{\partial x} = 0$$ ... (2.44d)

In Cathode GDL:

at z=Z_3 $$-K_c \frac{\partial T_i}{\partial z} = -K_m \frac{\partial T_i}{\partial z}$$ ... (2.45a)

at z=Z_4 $$-K_c \frac{\partial T_i}{\partial z} = h_c (T_\infty - T_i)$$ ... (2.45b)

at x=0 $$-K_c \frac{\partial T_i}{\partial x} = 0$$ ... (2.45c)

at x=X_1 $$-K_c \frac{\partial T_i}{\partial x} = 0$$ ... (2.45d)

In membrane:

at z=Z_2 $$-K_a \frac{\partial T_a}{\partial z} = -K_m \frac{\partial T_m}{\partial z}$$ ... (2.46a)

at z=Z_2 $$-K_m \frac{\partial T_m}{\partial z} = -K_C \frac{\partial T_C}{\partial z}$$ ... (2.46b)

at x=X_1 $$-K_m \frac{\partial T_m}{\partial x} = 0$$ ... (2.46c)

at z=L $$-K_m \frac{\partial T_m}{\partial x} = 0$$ ... (2.46d)

Boundary Conditions for the Gas Channels

In Anode Gas Diffusion Channel:

at z=0 $$\frac{\partial C_i}{\partial x}=0 \quad \ldots (2.47a)$$

at z=Z_1 $$-D_a \frac{\partial C_i}{\partial z}=K_a(C_\infty - C_i) \quad \ldots (2.47b)$$

In Cathode Gas Diffusion Channel:

at z=Z4 $$\frac{\partial C_i}{\partial x}=0 \quad \ldots (2.48a)$$

at z=Z5 $$-D_a \frac{\partial C_i}{\partial z}=K_a(C_\infty - C_i) \quad \ldots (2.48b)$$

Transport Losses

Activation Overpotential:

During both anode and cathode reactions, the losses due to the slowness of the reaction on the electrode surface are called activation overpotential. Activation overpotential is directly related to the rates of electrochemical reactions. In the next chapter the calculation of these losses is shown in flow charts. Some amount of energy needs to be given to the system for adding or removing electrons from the electrode.

This energy causes the decrease in the terminal voltage. The effect of this loss is more significant in the low current density regions as shown in Fig. 2.6.

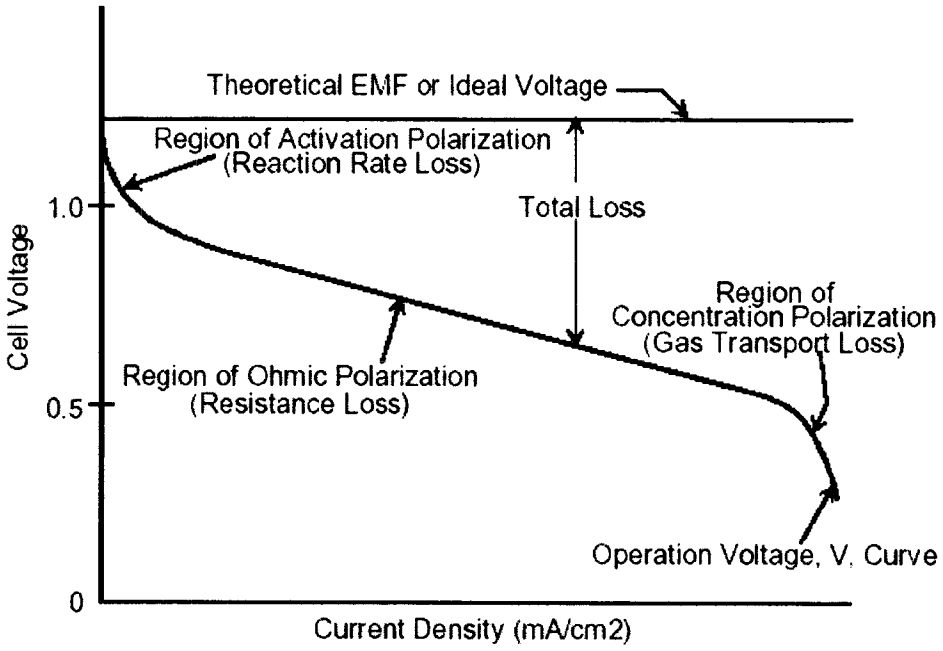

Figure 2.6. Description of Polarization Curve.

This kinetic or activation polarization loss can be found from the Tafel equation

$$\eta_{act} = b \ln\left(\frac{i}{i_0}\right) \qquad \ldots (2.49)$$

where

i=observed current density

b=Tafel slope

i_0=exchange current density

i_0 value is considered as constant i.e. catalytic parameters are assumed in this work.

Ohmic losses:

The decrease in the terminal voltage due to the opposition for the flow of electrons in the electrode and opposition to the flow of ions in the membrane is called Ohmic overpotential or Ohmic loss. These losses cause a linear drop of terminal voltage in the low and medium current density regions of the polarization curve. These losses are function of the thickness of the electrolyte. A thin electrolyte would be useful in reducing these losses. If a very thin electrolyte is used then intermixing of anodic and cathodic reactants might take place, which causes reduction in Faradaic efficiencies. These losses might contribute to the heat generated in high temperature fuel cells.

$$\dot{q}_{ohm} = i^2 r_i \qquad \ldots (2.50)$$

where

i = current density

r_i = resistance of the cell

Mass-transport losses:

At high current densities, a large amount of reactants should be provided. When the reactant concentration can not be increased anymore by the diffusion and convection process, losses occur. These losses, due to the unavailability of reactant concentration, are called Mass-transport or concentration overpotential. These losses can be calculated as

$$\eta_{Conc} = \frac{RT}{2F} \ln\left(1 - \frac{i}{i_L}\right) \qquad \ldots (2.51)$$

where

R=Universal gas constant

F=Faraday's constant

i=current density

i_L=limiting current density

CHAPTER 3

COMPUTATIONAL MODEL

This chapter aims to explain the techniques and approaches used to solve the mathematical model presented in the previous chapter and development of a computational code that implements the solution algorithms for simulating the tri-layer fuel cell. The computational model in this work utilizes a hybrid scheme that employs finite element discretization of the governing equations for the solid regions and finite difference discretization for the gas flow regions. The governing equations of heat and mass in the gas flow channels are discretized using a first order forward difference scheme. The finite element formulation for the transport equations in the solid involves the Galerkin-based weighted residual method. Computational domain for the tri-layer fuel cell is discretized into a finite element mesh consisting of four-noded rectangular elements as shown in Fig. 3.1. The flow regions of the gas channels are discretized into a one-dimensional finite difference grid. In order to have continuity, the finite difference nodes in the channels correspond to the nodes of the finite elements used in the solid regions.

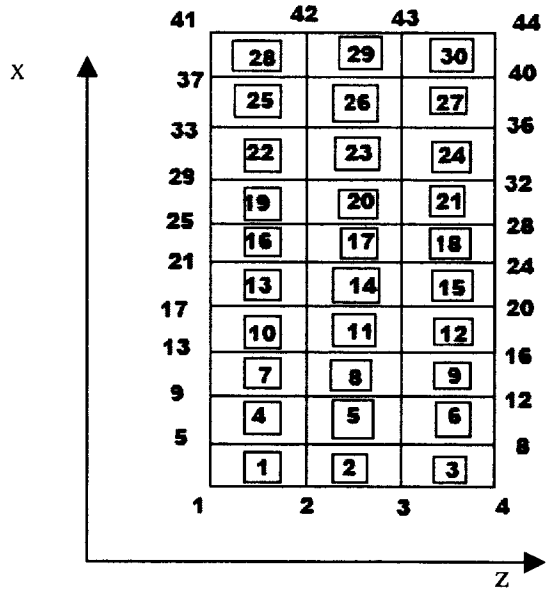

Figure 3.1. Schematic of Mesh.

A subroutine in the program is written to calculate all the node numbers and element numbers and save in different matrices. Depending upon the input data, the chemical equations are solved and the parameters like co-efficient of convection and co-efficient of diffusion of gases, velocities of gases, water and protons are calculated.

Flow Chart

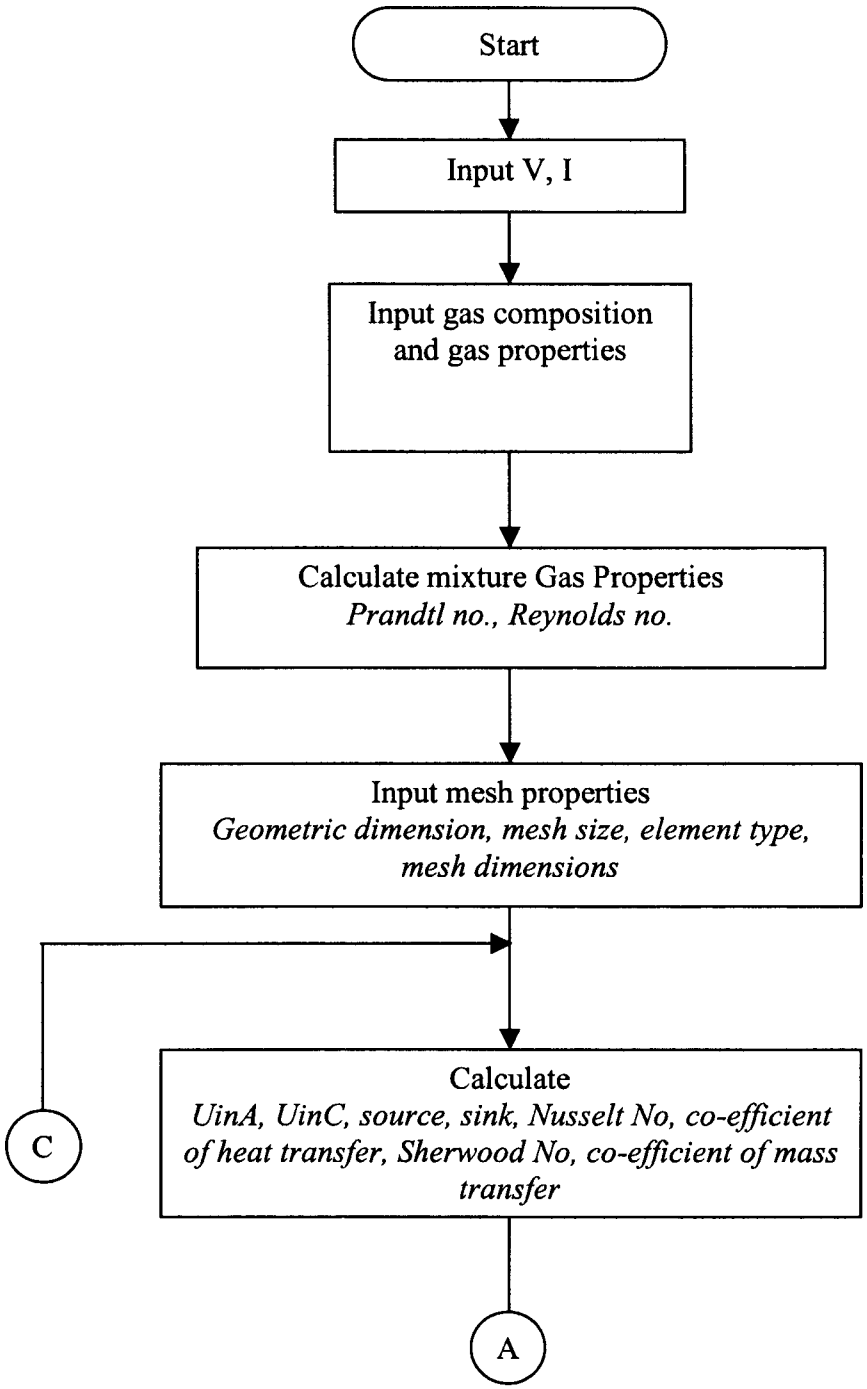
Start
Input V, I
Input gas composition and gas properties
Calculate mixture Gas Properties
Prandtl no., Reynolds no.
Input mesh properties
Geometric dimension, mesh size, element type, mesh dimensions
Calculate
UinA, UinC, source, sink, Nusselt No, co-efficient of heat transfer, Sherwood No, co-efficient of mass transfer
C
A

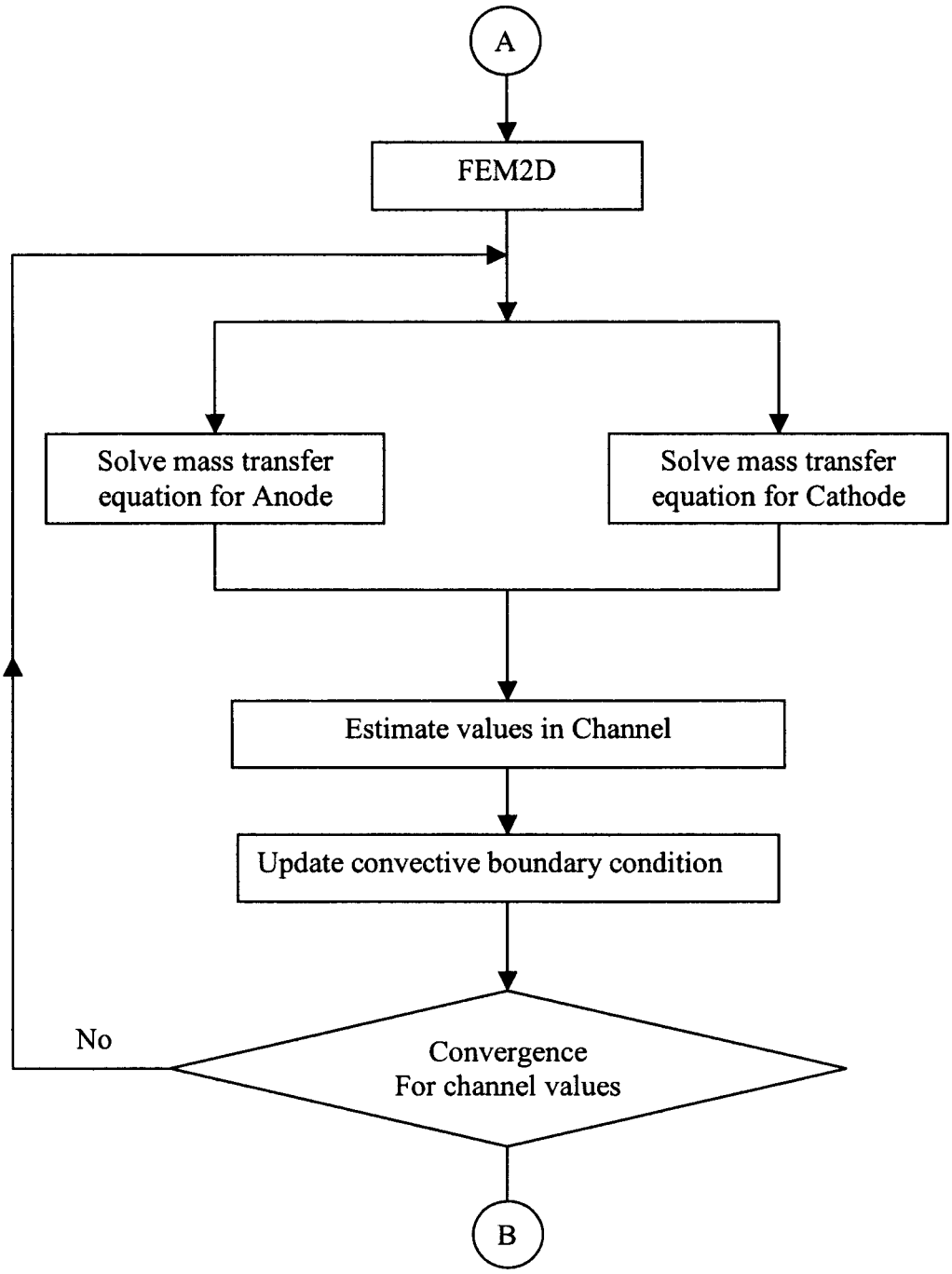
A
FEM2D
Solve mass transfer equation for Anode
Solve mass transfer equation for Cathode
Estimate values in Channel
Update convective boundary condition
No
Convergence For channel values
B

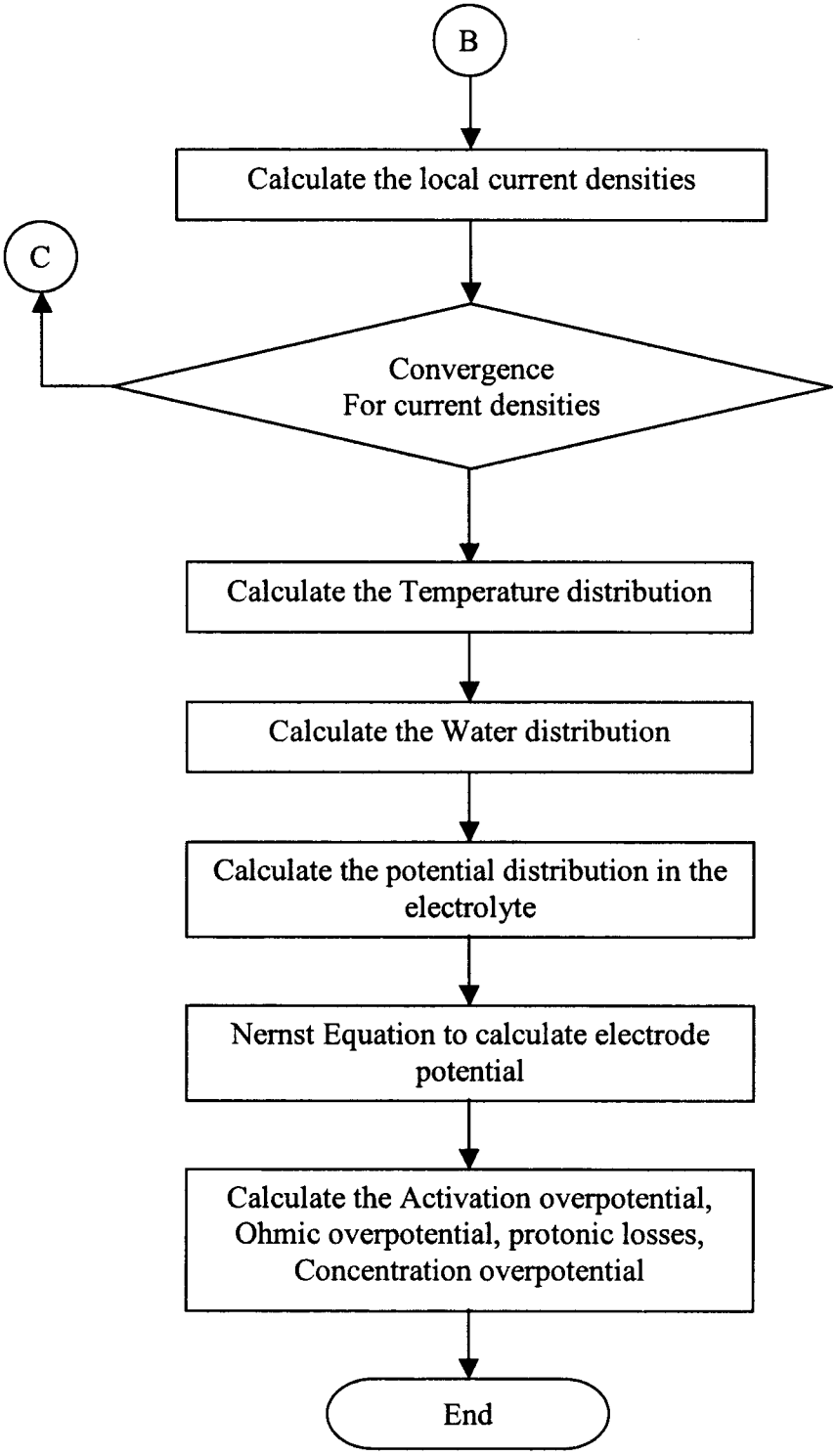
B
Calculate the local current densities
C
Convergence
For current densities
Calculate the Temperature distribution
Calculate the Water distribution
Calculate the potential distribution in the electrolyte
Nernst Equation to calculate electrode potential
Calculate the Activation overpotential, Ohmic overpotential, protonic losses, Concentration overpotential
End

Consideration of Convective and Diffusive Terms

The gases which flow through the gas channels diffuse through the porous gas diffusion layer. This effect is mathematically simulated by using a one-dimensional equation along the gas channel length.

$$U\frac{\partial C}{\partial x} = -K_x * (C - C_\infty)$$

This equation reduces a lot of computational time and simplifies the whole domain. The mesh along the gas channel is finely divided so that accurate results are obtained quickly. The above equation suggests that flow in the gas channel is divided into two parts. One part flows along the gas channel, whereas the other part allows for the diffusivity into GDL.

This equation is used to calculate the amount of gas concentration present along the gas channels. Initially the GDL is solved with constant concentration in the gas channels. This equation is then used to calculate the gas concentration present along the channel using the values of concentration in the neighboring nodes of GDL and initial velocity of gas flowing through the channel.

For convergence of values in the gas channel:

$$U * \left(\frac{C_{i+1} - C_i}{dxx} \right) = -k_{x,i-1} * (C_c - C_i)$$

On simplifying, we get

$$C_{i+1} = C_i * \left(\left(\frac{dxx * k_{x,i-1}}{U} \right) + 1 \right) - \left(\frac{C_c * dxx * k_{x,i-1}}{U} \right)$$

Schematic of Channel properties is shown in Fig. 3.2.

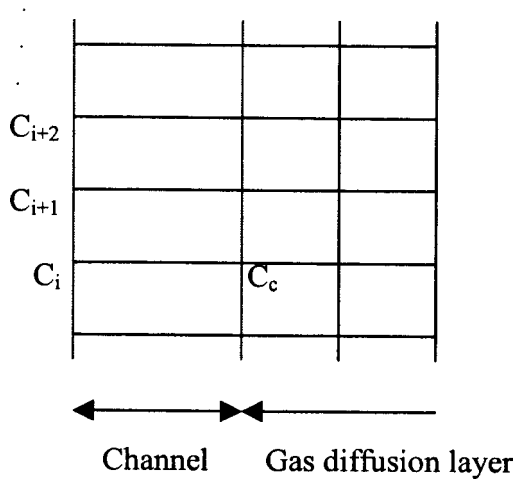

Figure 3.2. Schematic of Channel Properties.

In the above mesh, to calculate the value of C_{i+1} the equation explained above is used. The GDL is again solved with the new values of the concentration of gases present in the gas channel. This process of back substitution and solving is done until the error value is found less than 0.00009. The chart in Figure 3.3 shows the variation of error in the gas channel.

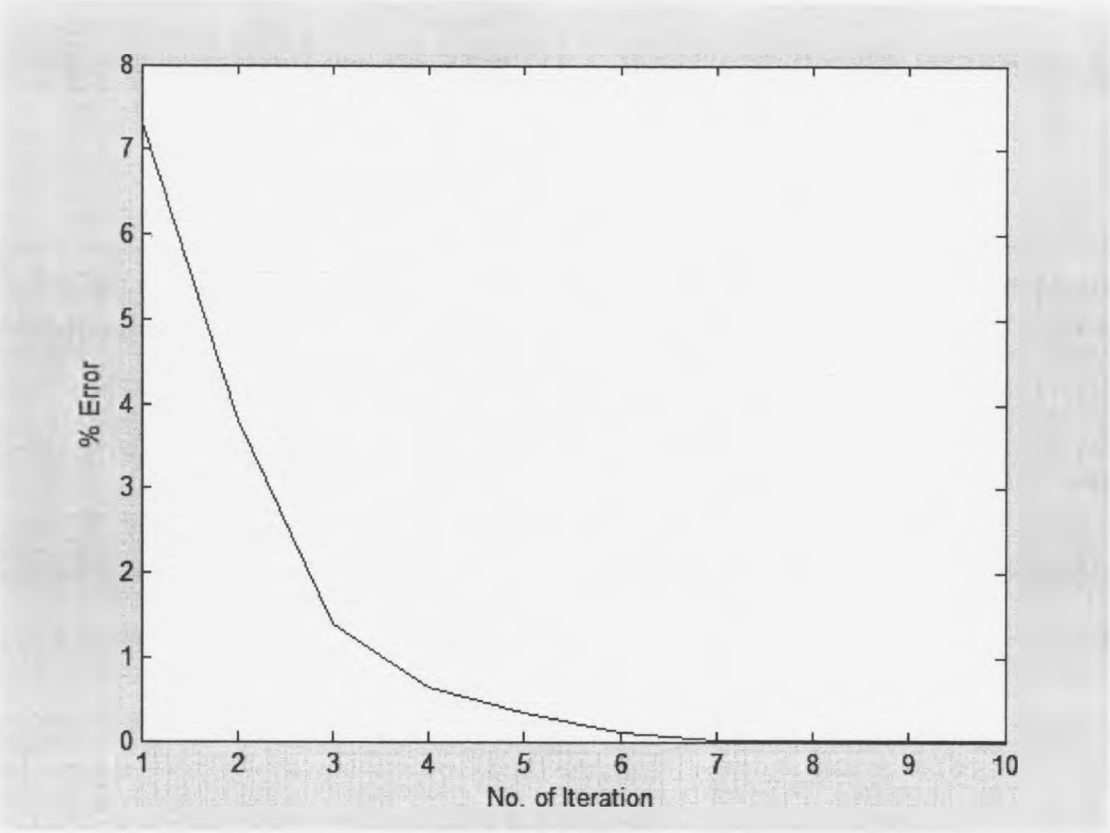

Figure 3.3. Convergence of values in Anode Gas Channel.

CHAPTER 4

RESULTS AND DISCUSSION

This chapter presents results for analyzing the performance of a tri-layer PEM fuel cell using the computational simulation model discussed in the previous chapters. Results and discussions are first given for a grid refinement study and a validation of the computational model. This is followed by a parametric study to evaluate the sensitivity of different operating conditions and electrode/membrane material parameters on the performance of fuel cells.

Operating and Modeling Parameters

The operating conditions, mixture gas compositions, electrodes, and membrane structural and physical properties that are used for the base case simulation are presented in Table 4.1. The temperature and pressure for a typical case are 70°F and 1 bar, respectively.

For this initial evaluation of the model parameters such diffusivities and conductivities are assumed as constant. For the validation studies, parameters are changed in order to match the experimental conditions and parameters.
Due to the unavailability of data, the base case conditions are assumed to be the same base case conditions as in Berning and Djilali's work [11].

Table 4.1.
Data for base case conditions

Anode diffusion layer

Property	Value
Thermal conductivity	0.455 W/m.K
Hydrogen Reference Concentration	56.4 mol/m3
Cathodic charge transfer co-efficient for anode reaction	1
Anodic charge transfer co-efficient for anode reaction	1
Gas diffusion layer thickness	0.26e-3 m
Electrode porosity	0.4
Hydrogen Concentration Parameter	0.25
Anode reference exchange current density	1.4 e11 A/m3
Electrode Hydraulic permeability	4.73e-19 m2
Initial Current Density	2e4 A/m3
Temperature	300 K
Initial Concentration	35e5 mol/m3
Diffusion Co-efficient	3.66e-5

Membrane Layer

Material Property	Value
membrane conductivity	1.3 W/m.K
Membrane thickness	0.23e-3 m
Membrane porosity	0.28
Electrode Hydraulic permeability	4.73e-19 m2
Diffusion Co-efficient	4.5e-9

(Continued on following page)

Table 4.1 (continued)

Cathode Diffusion Layer

Material Property	Value
Thermal conductivity	1.3 W/m.K
Oxygen Reference Concentration	3.39 mol/m3
Cathodic charge transfer co-efficient for cathode reaction	2
Anodic charge transfer co-efficient for cathode reaction	2
Gas diffusion layer thickness	0.26e-3 m
Electrode porosity	0.4
Oxygen Concentration Parameter	0.25
Cathode reference exchange current density	10 A/m3
Electrode Hydraulic permeability	4.73e-19 m2
Initial Current Density	2e4 A/m3
Temperature	300 K
Initial Concentration	35e5 mol/m3
Diffusion Co-efficient	8.8e-6

Mesh Refinement Study

In order to ensure the accuracy of the computational model with respect to the size of the element, a mesh refinement study is conducted. Mesh was refined both in the flow direction (x –direction) of the channel as well as along the thickness of the tri-layers (z –direction). A summary of this mesh independent study is given based on the flowing progressively refined grid: 9 X 10, 9 X 20, 18 X 20, 18 X 40 and 36 X 40. The tolerance limit for convergence was set to 10^{-6}.

Fig. 4.1 and Fig. 4.2 show distribution of hydrogen and oxygen gas concentrations in the anode and cathode gas diffusion layers, respectively. In these regions the mesh size in the z-direction is fixed as 18 and mesh size in the x - direction is varied from 10 to 40. As we can see, with the refinement of mesh size, the distributions in the both layers change and converge progressively to the case with 18 x 40. The percent relative errors listed in Table 4.2 and Table 4.3 show that the percent relative errors decrease with reduced mesh sizes.

Fig. 4.3 and Fig. 4.4 show mesh refinement for concentration distribution in the anode and cathode gas channels, respectively. For these cases, the mesh size in z - direction is fixed as 18 along GDL and 10, 20 and 40 in x - direction. Results for gas concentrations are presented in Table 4.4 and Table 4.5, which show a converged solution for the mesh 40 X 18.

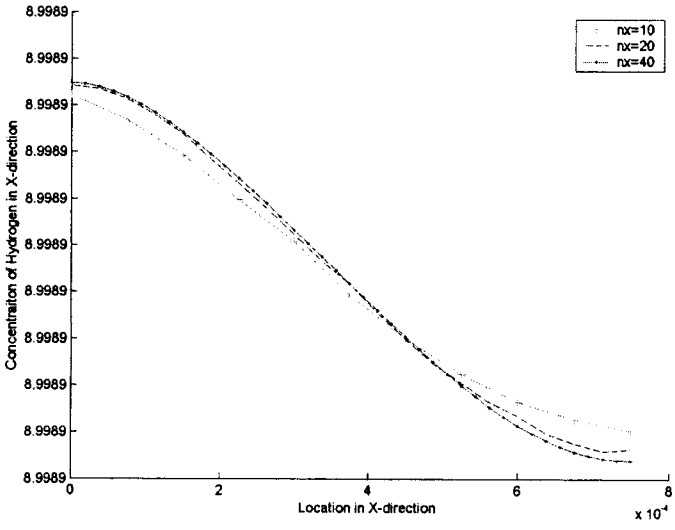

Figure 4.1. Mesh refinement in X-direction in Anode GDL.

Table 4.2.

Data for mesh refinement in Anode GDL

Nx=10; Nz=6	Nx=20; Nz=6	% Error	Nx=40; Nz=6	% Error
8.99891	8.998911	4.44E-08	8.998911	1.11E-08
8.998909	8.998910	1.00E-07	8.998910	1.11E-08
8.998908	8.998909	1.00E-07	8.998909	1.11E-08
8.998906	8.998907	7.86E-08	8.998907	2.22E-08
8.998904	8.998904	3.33E-08	8.998905	2.22E-08
8.998902	8.998902	5.00E-08	8.998902	0.00E+00
8.998900	8.998900	0.00E+00	8.998900	1.11E-08
8.998899	8.998898	4.44E-08	8.998898	1.11E-08
8.998897	8.998897	6.67E-08	8.998896	4.44E-08
8.998897	8.998896	1.18E-07	8.998895	3.78E-08
8.998896	8.998895	8.89E-08	8.998895	5.56E-08

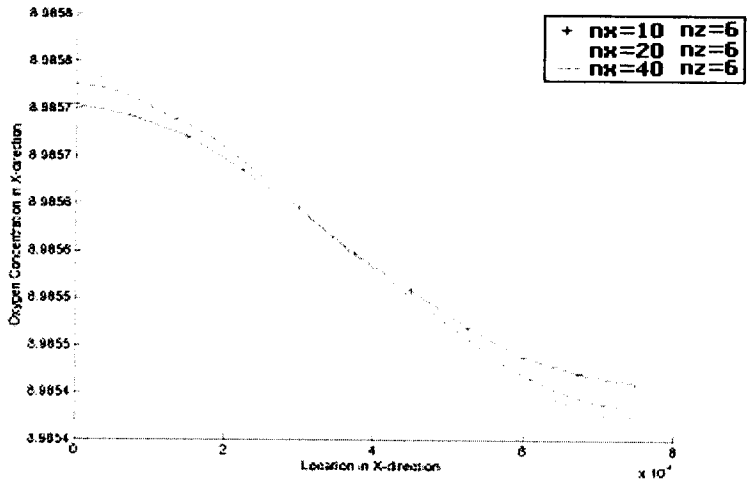

Figure 4.2. Mesh refinement in X-direction in Cathode GDL.

Table 4.3

Data for mesh refinement in Cathode GDL

Nx=10; Nz=6	Nx=20; Nz=6	% Error	Nx=40; Nz=6	% Error
8.985755	8.985776	2.34E-06	8.985786	1.11E-06
8.985742	8.985762	2.23E-06	8.985772	1.11E-06
8.985721	8.985734	1.45E-06	8.985739	5.56E-07
8.985685	8.985694	1.05E-06	8.985694	0.00E+00
8.985645	8.985645	0.00E+00	8.985645	0.00E+00
8.985598	8.985596	2.23E-07	8.985594	2.23E-07
8.985558	8.985550	8.90E-07	8.985543	7.79E-07
8.985519	8.985507	1.34E-06	8.985497	1.11E-06
8.985488	8.985468	2.18E-06	8.985458	1.11E-06
8.985470	8.985443	2.95E-06	8.985433	1.11E-06
8.985460	8.985435	2.79E-06	8.985425	1.11E-06

The mesh refinement study clearly shows that a mesh size of 18 x 40 would be sufficiently refined mesh for converged numerical solution for the simulation model. Rest of the simulation study, therefore, is carried out based on this mesh size distribution.

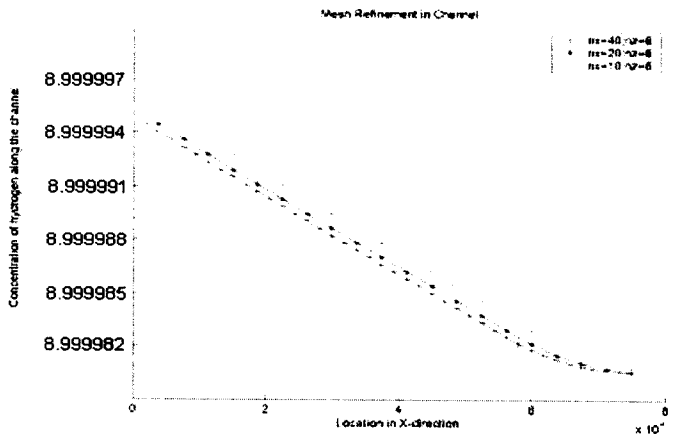

Figure 4.3. Mesh refinement in Anode Gas Channel.

Table 4.4.

Data for mesh refinement in Anode Gas Channel

Nx=10 Nz=6	Nx=20 Nz=6	% Error	Nx=40 Nz=6	% Error
8.999996	8.999994	1.53E-05	8.999994	8.69E-06
8.999993	8.999991	1.65E-05	8.999991	6.33E-06
8.999990	8.999989	1.49E-05	8.999988	7.70E-06
8.999987	8.999986	1.52E-05	8.999985	7.58E-06
8.999985	8.999983	1.51E-05	8.999983	7.55E-06
8.999982	8.999981	1.51E-05	8.99998	7.54E-06
8.999979	8.999978	1.50E-05	8.999977	7.49E-06
8.999977	8.999975	1.47E-05	8.999975	6.12E-06
8.999974	8.999973	8.68E-06	8.999973	3.25E-06
8.999973	8.999973	2.90E-06	8.999973	3.67E-07

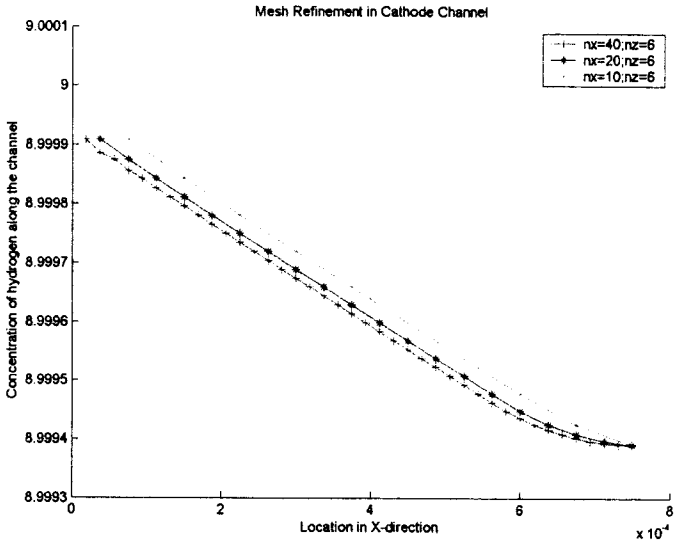

Figure 4.4. Mesh refinement in Cathode Gas Channel.

Table 4.5.

Data for mesh refinement in Cathode Gas Channel

Nx=10; Nz=6	Nx=20; Nz=6	%Error	Nx=40; Nz=6	% Error
8.999908	8.999875	3.68E-04	8.999856	2.08E-04
8.999843	8.999812	3.46E-04	8.999796	1.72E-04
8.999781	8.999750	3.39E-04	8.999735	1.70E-04
8.999720	8.999690	3.38E-04	8.999674	1.69E-04
8.999659	8.999629	3.37E-04	8.999614	1.69E-04
8.999598	8.999568	3.37E-04	8.999553	1.68E-04
8.999538	8.999508	3.34E-04	8.999493	1.67E-04
8.999478	8.999448	3.23E-04	8.999436	1.36E-04

(continued on following page)

Table 4.5 (continued)

Nx=10; Nz=6	Nx=20; Nz=6	%Error	Nx=40; Nz=6	% Error
8.999425	8.999408	1.93E-04	8.999402	7.23E-05
8.999391	8.999391	0.00E+00	8.999390	8.15E-06

Validation of Simulation Model

The accuracy of the simulation model is tested by comparing the results with a number of previous numerical studies conducted by Berning and Djilali [11], and experimental studies performed by Ticianelli et al. [10] and Kim et al. [8]. The operating conditions and parameters are changed in order to simulate the case similar to their studies. However, there remains some uncertainty in a few of the selected operating conditions, parameters and sizes of the fuel cell, as they are not reported in those studies. The results obtained by this computational model are observed to be satisfying the previous work done.

Comparison with Berning and Djilali [11]

The base case is initially compared with Berning's data. The comparison of results with Berning and Djilali is shown in Fig. 4.5.

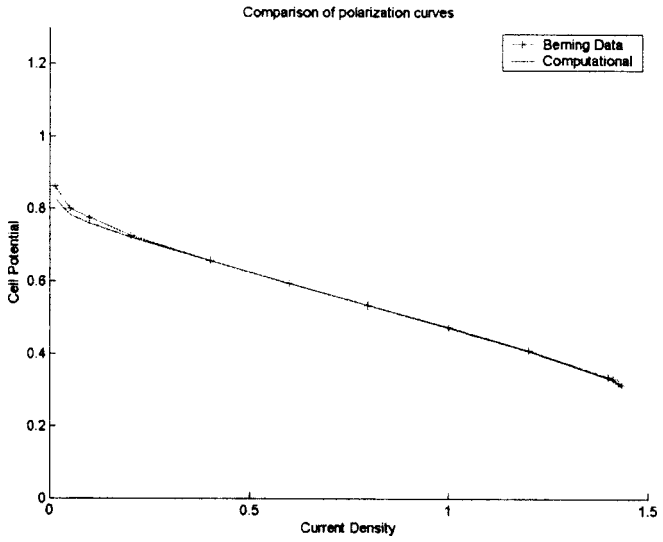

Figure 4.5. Comparison with Berning and Djilali's [11] model.

Results displayed in Fig. 4.5 and Table 4.6 show a close prediction as that given by Berning's model, particularly in intermediate ranges of current density. The operating conditions, type and size of the tri-layer fuel cell used for the comparison study is given in Table 4.7.

Table 4.6.

Data for Validation with Berning's work [11]

Current Density (A/m^2)	Voltage (Volts)		% Error
	Computational	Berning Data	
0.01293	0.811252	0.862774	6.350838
0.09914	0.759168	0.775182	2.109464
0.20259	0.720673	0.727007	0.878962
0.40086	0.656209	0.656934	0.110507
0.59914	0.595211	0.596861	0.277305
0.79741	0.535152	0.534927	0.042021
1.00000	0.473486	0.475613	0.449289
1.20259	0.409666	0.412299	0.642892
1.40086	0.335131	0.337226	0.625121
1.41379	0.327864	0.332847	1.519688
1.42672	0.318949	0.319708	0.237957
1.43535	0.310975	0.315328	1.39996

There is some deviation in the current density region 0 - 100 $mAmp/cm^2$. These losses explain that the activation overpotential calculated in this computational model is a little higher than that given by Bernings's model.

Table 4.7

Base case conditions for Berning's and Djilali's work

Property	Value
Electrode thickness	0.26×10^{-3} m
Membrane thickness	0.23×10^{-3} m
Inlet fuel and air temperature	80 °C
Gas phase electrode porosity	0.4
Electronic Conductivity	6000 S/m
Effective Thermal Conductivity	75 W/mK
Protonic diffusion co-efficient	4.5×10^{-9} m^2/s^2
Thermal Conductivity of Membrane	0.67 W/mK
Heat Transfer Co-efficient between gas and solid phase	7.0×10^5 W/m^2

Comparison with Ticianelli et al. [10]

The computational model is next compared with the experimental work conducted by Ticianelli et al. [10]. Their primary effort was to improve the performance of the PEM fuel cell with Platinum loading of the order of $0.34 mg/cm^2$ that is significantly reduced from then state-of-the art electrodes and platinum loading ($4 mg/cm^2$). Their fabricated electrodes were impregnated with a certain amount of Nafion and platinum loading of $0.34 mg/cm^2$. Such a design primarily created a three-

dimensional reaction zone, and hence more effective utilization of Platinum loading. The electrochemically active area of the electrodes was evaluated by cyclic voltammetry. The polarization curve was correlated in the form of an empirical equation, but neglecting higher current density range where the mass transportation losses are predominant. The data selected from their study and used in this comparison study is listed in Table 4.8.

Table 4.8

Base case conditions for Ticianelli's work

Cell no.	E_0 (V)	$i_0 \times 10^9$ (A/cm^2)	b (V/dec)
PEM 3, GE/HS-UTO	0.924	166	0.068
PEM 3, M&E assembly	0.950	20	0.055
PEM 5, PE, 2%	0.721	23	0.099
PEM 23, PE, 2%	0.912	3	0.055
PEM 21, PE, 3.3%	0.933	110	0.072
PEM 27, PE, 5%	0.930	6	0.055
PEM 32, PE, 10%	0.955	17	0.055
PEM 45, PE, 4%	0.882	4	0.0566

The above comparison includes the appropriate electro kinetic parameters for their designed electrodes.

The comparison of results is shown in Fig. 4.6 and Table 4.9. Results show very close prediction with the experimental data, including the low current density

Table 4.9

Data for Validation with Ticianelli's work

Current Density (mA/m^2)	Voltage (Volts)		% Error
	Computational	Ticianelli	
0.1	1.006013	1.012	0.59516
0.2	0.96164	0.965928	0.445932
0.3	0.925274	0.928602	0.359598
0.4	0.892187	0.894856	0.299096
0.5	0.860897	0.863072	0.25268
0.6	0.830743	0.832529	0.215094
0.7	0.801372	0.802843	0.183525
0.8	0.772576	0.773784	0.156291
0.9	0.744218	0.745203	0.132303
1.0	0.716206	0.717	0.110813
1.1	0.688474	0.689103	0.091284
1.2	0.660973	0.661457	0.073313
1.3	0.633665	0.634024	0.056586
1.4	0.606523	0.606771	0.040853

regions where the maximum error is found to be within 0.6%.

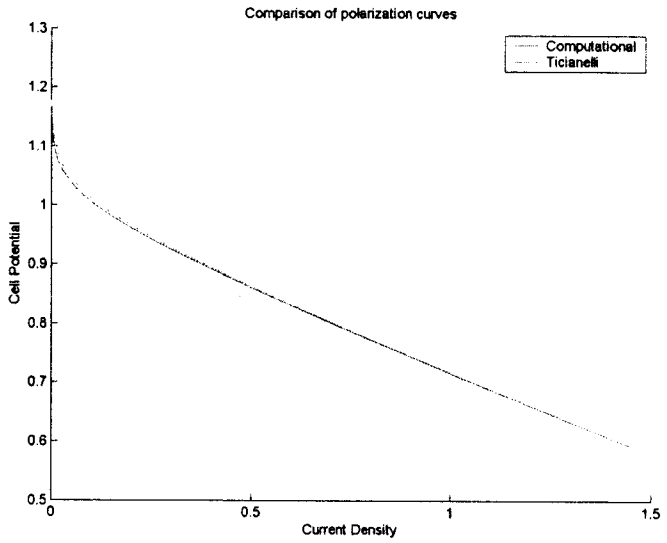

Figure 4.6. Comparison with Ticianelli's work [10].

Comparison with Kim et al. [8]

The computational model is also compared with the experimental results of Kim et al [8]. Their work took an extra step in calculating the voltage at higher current densities incorporating the mass transportation losses, which is one of the major problems in effective use of fuel cells for power generation. Their fabricated electrode – electrolyte fuel cell consists of integrated catalyst and gas diffusion layer impregnated with Nafion solution and Nafion 115 membrane. The Nafion-impregnated electrodes had a Platinum loading of $0.4mg/cm^2$ and a Nafion content of $0.6mg/cm^2$. Cell potential vs. current density were carried out with pure Hydrogen and Oxygen. The flow rates had a stoichiometric ratio of 1.2 on the fuel side and 2.0

on the oxidant side. Table 4.10 lists all operating parameters used for this comparison study. Simulation results along with Kim's experimental data are presented in Table 4.11 and Fig. 4.7. The simulation model again closely predicted the cell potential losses in low to intermediate ranges of current densities. However, the simulation model significantly under-predicted the cell potential losses due to mass transport losses at higher current densities. The decrease in cell potential in this range of current density is seen to be more abrupt than given by the experiments. This discrepancy may be caused by the lack of structural details such as pore size distribution available for fuel cell fabricated by Kim et al [8] and inadequate modeling of H^+ conductivity as a nonlinear function water concentration.

Table 4.10

Base case conditions for Kim's work

Pressure (Atm)	E_0 (mV)		b (mV/dec)		R ($\Omega.cm^2$)		m (mV)	N (Cm^2/mA)
	Eq 1	Eq 5	Eq 1	Eq 5	Eq 1	Eq 5	Eq 5	Eq 5
1	942	943	61	62	0.390	0.363	0.38	1.02×10^{-2}
2	973	978	57	60	0.434	0.363	2.90	5.72×10^{-3}
3	987	991	55	57	0.472	0.404	3.08	5.59×10^{-3}

The closeness in the lower and medium current density regions show the accuracy of the model in calculating the current density and other parameters.

Table 4.11

Data for Validation with Kim's work

Current Density (mA/m^2)	Voltage (Volts)		% Error
	Computational	Kim	
0.05	0.821868	0.820605	0.153738
0.10	0.792878	0.788102	0.602319
0.15	0.767212	0.762618	0.59876
0.20	0.742481	0.739303	0.42803
0.25	0.717842	0.716346	0.208404
0.30	0.692813	0.692593	0.031803
0.35	0.66700	0.666989	0.001715
0.40	0.639989	0.638349	0.256202
0.45	0.611259	0.605196	0.991882
0.50	0.580056	0.565582	2.495308
0.55	0.545165	0.516892	5.186114
0.60	0.504338	0.455565	9.670632
0.65	0.452569	0.376734	16.756483
0.70	0.373925	0.273724	26.797175

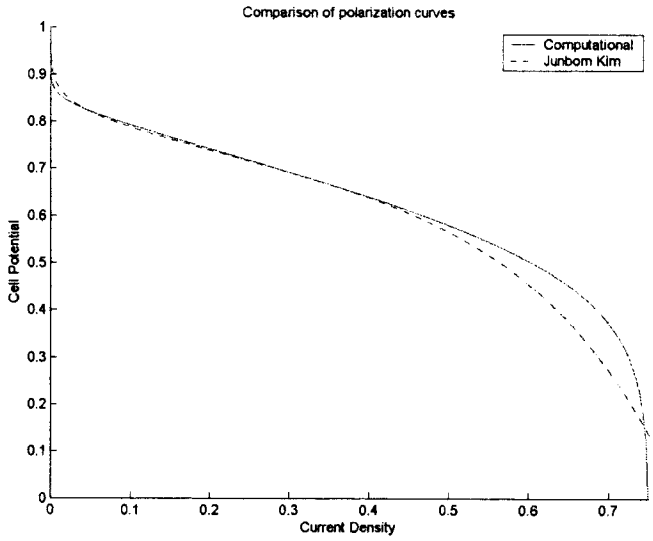

Figure 4.7. Comparison with Kim's work [8].

Simulated Fuel Cell Performance

The values of parameters chosen for the base case results are shown in Table 4.1. The base case results are broadly classified as flow of reactant gases in anode and cathode channels; flow of reactant gases in anode and cathode gas diffusion layers; water and temperature distribution in the anode-electrolyte-cathode region; and potential distribution in the electrolyte of the fuel cell.

The distribution of hydrogen in the anode gas diffusion layer is shown in Fig. 4.8 and the distribution of oxygen in the cathode gas diffusion layer is shown in Fig. 4.9.

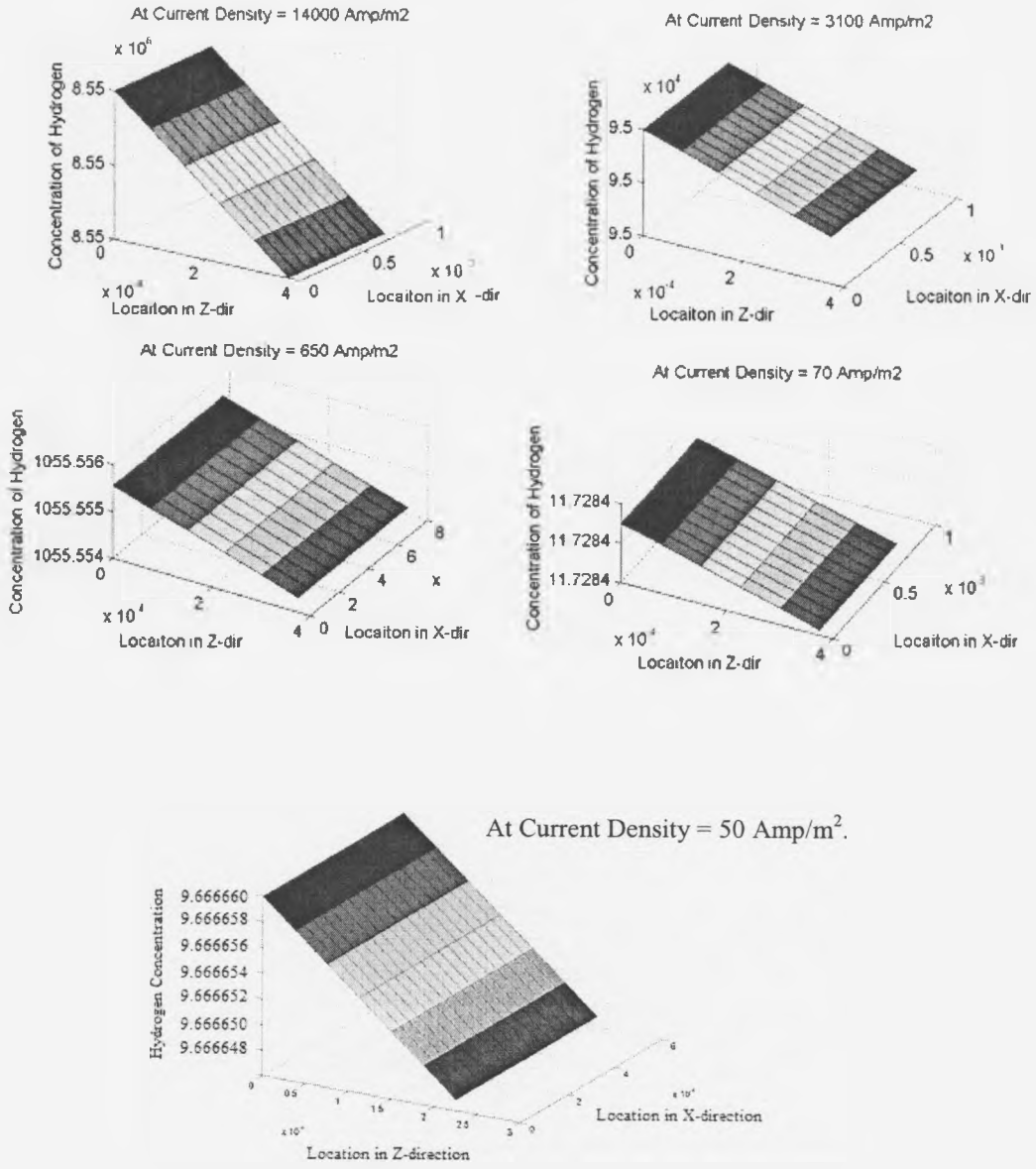

Figure 4.8. Hydrogen Concentration in Anode GDL.

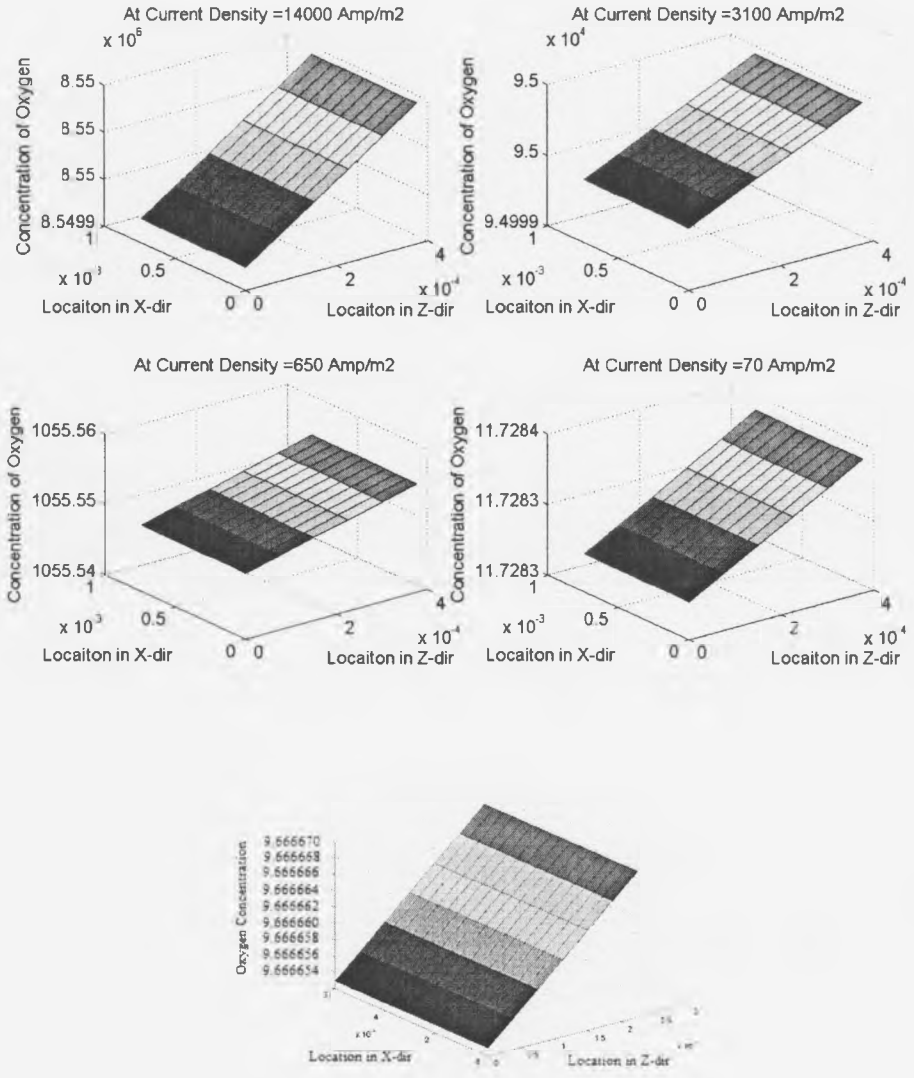

Figure 4.9. Oxygen Concentration in Cathode GDL.

Distribution of local current density along the channel is also calculated. The variation of current density along channel is important since it affects the average current density and the power output.

Distribution of potential in the Membrane:

The boundary conditions explained in the previous chapter clearly state that the potential would increase from anode side to cathode side. The change in voltage drop was found to be linear in the z-direction, whereas a curvilinear fashion was observed in the x-direction. The variation of voltage losses from X=0 to X=C_L is plotted at various positions of Z. These variations are shown in Fig. 4.10.

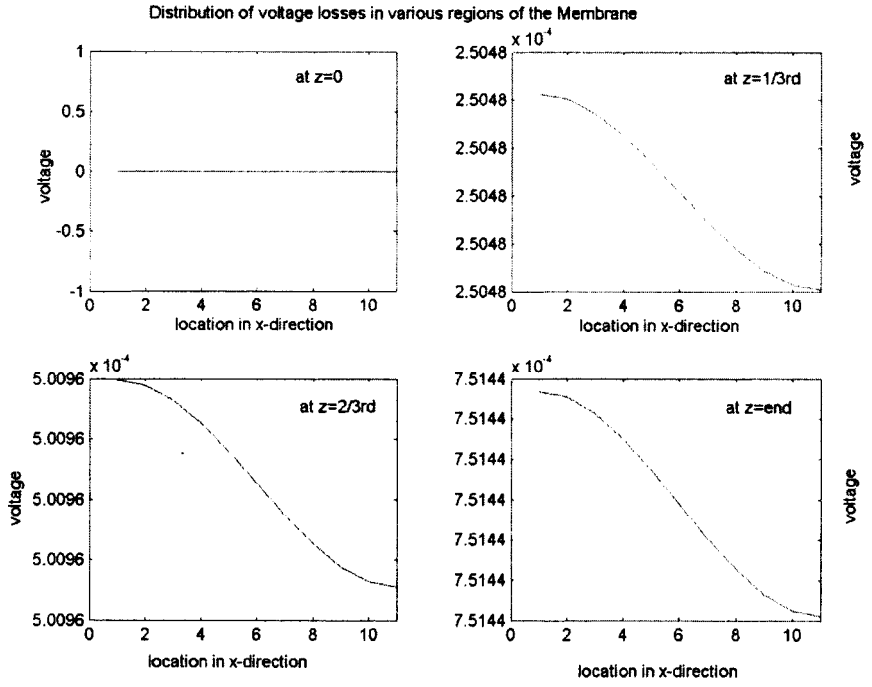

Figure 4.10. Distribution potential at different locations along X-direction in the membrane.

The equations for the potential distribution as discussed in previous chapters are solved in the membrane region. The potential distribution in the membrane is shown in Fig. 4.11.

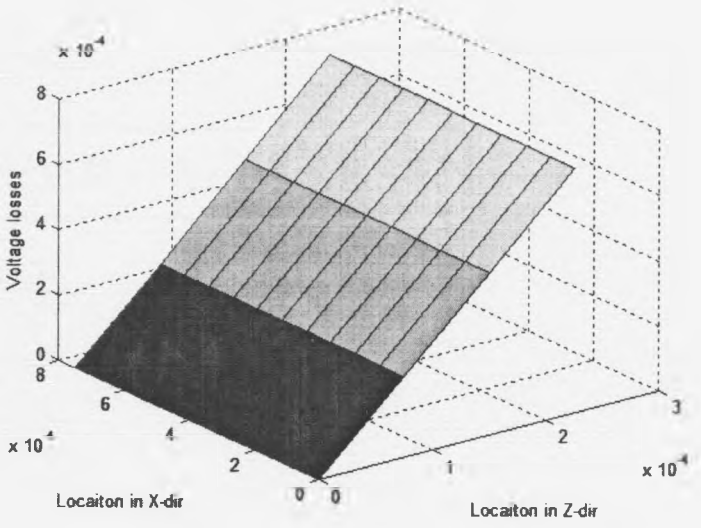

Figure 4.11. Potential Distribution in Membrane.

Distribution of Hydrogen gas along the anode gas channel:

The concentration of H_2 gas was found to be decreasing along the z-direction. The variation of H_2 gas along the gas channel was attributed to the variation of local current density. The contour plot in Fig. 4.12 shows the distribution of H_2 gas along the z-direction.

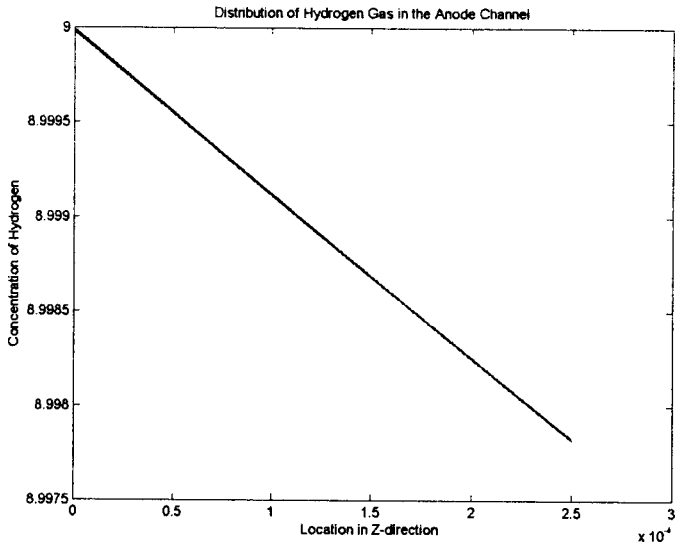

Figure 4.12. Distribution of Hydrogen gas in the Anode Channel.

Distribution of Oxygen gas along the cathode gas channel:

The concentration of O_2 gas is found to be increasing along the positive direction of Z. The contour plot shows the distribution of O_2 gas in the cathode gas diffusion layer. The effect of sink at the cathode catalyst layer tends to attract the available O_2 and convert into O^{2-} ions to react with the H^+. The distribution of Oxygen in the cathode GDL is shown in Fig. 4.13.

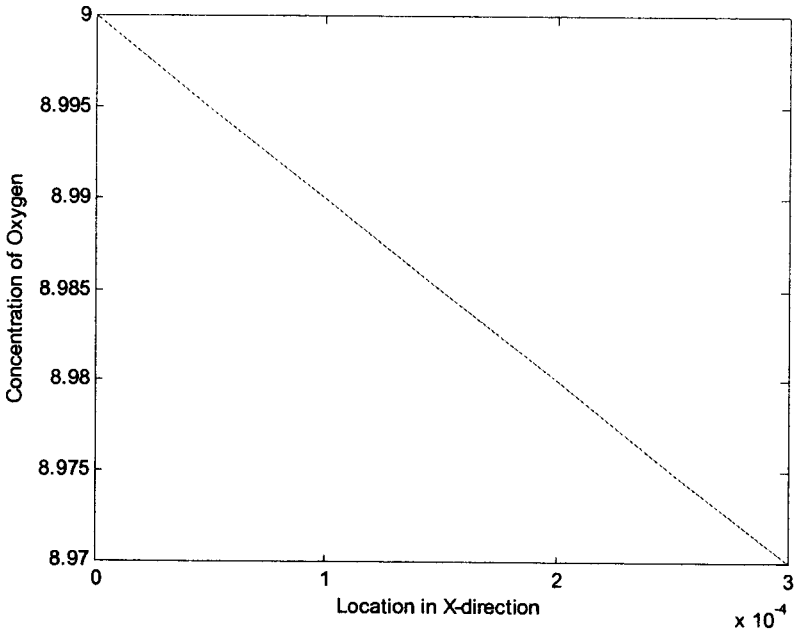

Figure 4.13. Distribution of Oxygen gas in the Cathode Channel.

Distribution of current density at the interface region:

The variation of the current density along the flow direction depends on the concentration of H^+ and O^{2-} ions present at the interface region. The variation of the current density at the interface region is shown in Fig. 4.14.

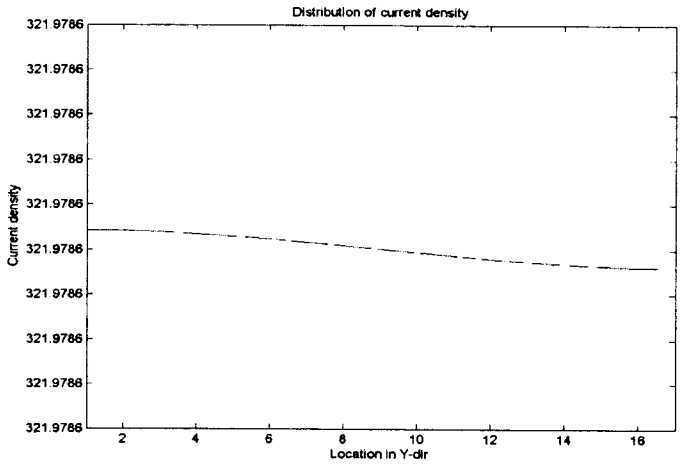

Figure 4.14. Distribution of current density along flow direction.

Parametric Study

This section illustrates the importance of individual parameters of the fuel cell. A single parameter is varied over a range and the performance of fuel cell is studied. The parameters studied in this study are pressure, and electrode material and Nafion loading. The parametric study is helpful in understanding the role of each individual component. A combination of all the optimized conditions obtained from the parametric study would be very helpful to analyze the best operating conditions of the cell.

Effect of Operating Pressure

The operating pressure of the pressure of the reactant gases in the channels is varied and the results were studied in terms of polarization curves. The effect of pressure can be attributed to the variation of several transport and thermodynamic properties. This includes (i) inlet gas composition assuming the inlet gasses as fully

humidified; (ii) reference potential, E_o as given by the Nernst equation; (iii) exchange current density, i_o; and (iv) Binary diffusion coefficient. In this study the effects of item (i) and (ii) are incorporated. Fig. 4.15 shows polarization curves with increase in operating pressure. Results show that overall performance in terms of activation losses, Ohmic losses and mass diffusion improved with increase in pressure. However, the effect is less significant at higher pressures. Several detail observations can also be made. It can be noticed that initial drop in the potential decreased with increasing in pressure, indicating a decrease in activation losses. The ohmic loss also decreases as evident by the decrease in the slope of the linear part of the polarization curve. Further, there is a significant increase in limiting current density, indicating a decrease in mass diffusion losses with increased pressure.

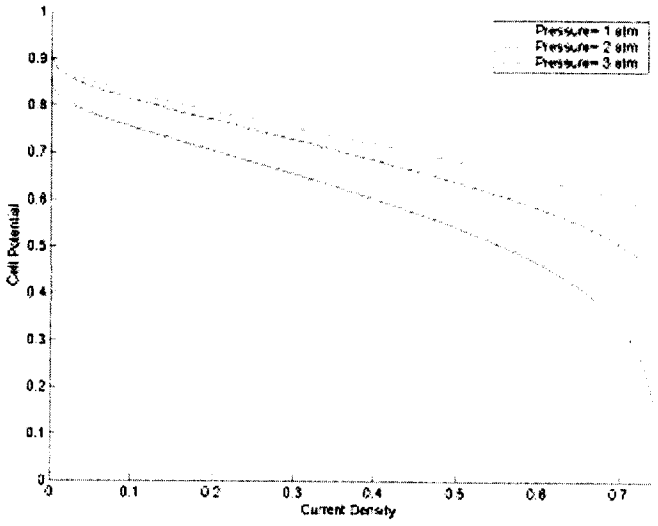

Figure 4.15. Effect of pressure on cell performance.

Comparison electrode designs with different platinum loading

Two different electrode designs are evaluated using the simulation model. The design – 1is the GE/HS-UTC , which is a single cell membrane electrode containing a platinum loading of $4mg/cm^2$. The second design (M&E), proposed and fabricated by Ticianelli et. al. [6] consists of Nafion membrane and a Nafion-impregnated electrode containing $0.35mg/cm^2$. The kinetic data for this design with varying Nafion loading was obtained experimentally by Ticianelli et. al. [6] and presented in Table 4.8.

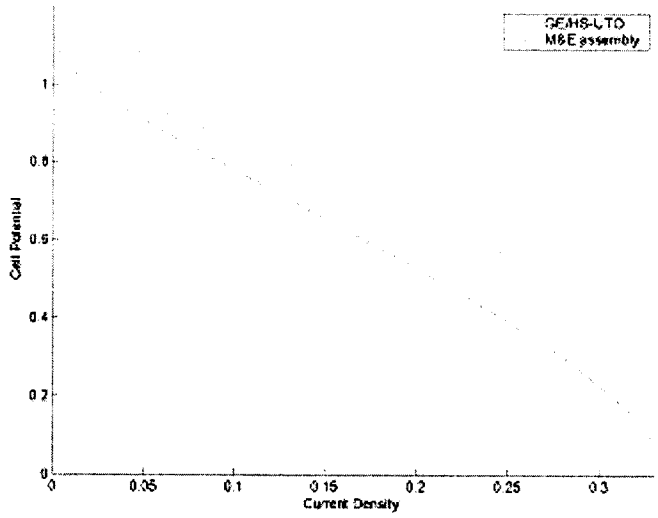

Figure 4.16. Performance of different membrane-electrode assembly designs.

Results presented in Figure 4.16 show that the Nafion-impregnated M&E design with one-tenth of platinum loading achieves similar level of activation loss as with the higher Platinum loading GE/HS-UTC design. Also, the M&E design shows improved performance in the intermediate range of current density.

Effect of Nafion loading:

Nafion loading in the Nafion-impregnated electrode increases the active reaction area, and thus gives improved reaction rates. However, with increased Nafion loading the electrodes becomes thicker and give rise to increased mass transport losses. Simulation is carried out with varying Nafion loading (2% - 10%) and results are presented in Figure 4.17. Results show that initially the performance increases with increase in Nafion loading. The performance of the cell showed improvement as the loading is increased up to 3.3%. With further increase in the loading, the performance deteorates, and hence indicates need for optimizing the percent of Nafion loading in Nafion-impregnated electrodes.

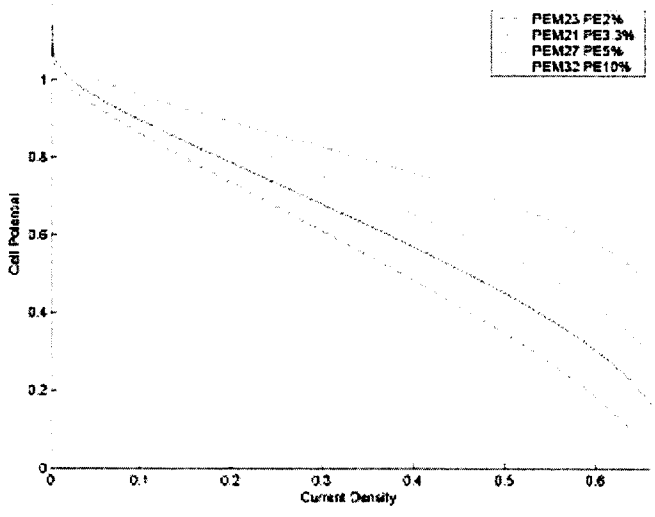

Figure 4.17. Effect of Nafion loading in Nafion-impregnated electrode

CHAPTER 5

CONCLUSIONS

A two-dimensional finite-element-based computer code is developed to evaluate the fuel cell system performance. A solution algorithm integrating the thermodynamics of electro-chemical reactions and solution transport equations are implemented into a computer code.

The model correlates well with the available data in the literature in the low to intermediate range of current densities.

A sensitivity study is conducted to evaluate the performance of the cell with varying operating pressure and electrode designs.

REFERENCES

[1]. T. E. Springer, T. A. Zawodzinski, G. Gottesfeld (1991) Polymer Electrolyte Fuel Cell Model, *Journal of Electrochemical Society,* vol. 138, pp. 2334-2342.

[2]. T.E Springer, M.S. Wilson and S. Gottesfeld (1993) Modeling and Experimental Diagnostics in PEMFC, *Journal of Electrochemical Soc.*, vol.140, pp. 3513–3526.

[3]. Dawn M. Bernardi and Mark W. Verbrugge (1992) A Mathematical Model of the Solid-Polymer-Electrolyte, *Journal of Electrochemical Society,* vol. 139(9), pp. 2477-2491.

[4]. Junbom Kim, Seong-Min Lee, Supramaniam Srinivasan (1995) Modeling of proton exchange membrane fuel cell performance with an empirical equation, *Journal of the Electrochemical Society*, vol. 142, pp. 2670 -2674.

[5]. Vladimir Gurau, Sadik Kakac, Hongtan Liu (1998) Mathematical Model for Proton Exchange Membrane Fuel Cells, Proceedings of the ASME Advanced Energy Systems Division, AES-Vol. 38, pp. 205-214.

[6]. E.A. Ticianelli, C.R. Derouin, A. Redondo, S.Srinivasan (1998) Methods to Advance Technology of Proton Exchange Membrane Fuel Cells, *Journal of Electrochemical Society*, vol. 135, pp. 2209-2214.

[7]. S. Dutta, S. Shimpalee, J. W. Van Zee (2000) Three-dimensional numerical simulation of straight channel PEM Fuel Cells, *Journal of Applied Electrochemistry,* vol. 30, pp. 135-146.

[8]. K. Dannenberg, P. Ekdunge, G. Lindbergh (2000) Mathematical model of the PEMFC, *Journal of Applied Electrochemistry*, vol. 30, pp. 1377-1387.

[9]. T. Berning, D.M. Lu, N. Djilali (2002) Three-dimensional computational analysis of transport phenomena in a PEM Fuel Cell, *Journal of Power Sources*, vol. 106, pp. 284-294.

[10]. T. Berning and N. Djilali (2003) Parametric Study of Transport phenomena in PEM Fuel Cells using a 3D Computational model, *ASME-1718*, pp. 187-194.

[11]. Zhiwen Ma, S.M Jeter, S.I Abbel-Khalik (2003) Numerical Simulation of the Molten Carbonate Fuel Cell performance under different Operating Conditions, *Proceedings of the ASME Summer Heat Transfer Conference*, vol. 2003, pp. 213 -219.

[12]. Datong Song, Qianpu Wang, Zhongsheng Liu, Titichai Navessin, Michael Eikerling, Steven Holdcroft (2004) Numerical Optimization study of the catalyst layer of PEM fuel cell cathode, Journal of Power Sources, vol. 126, pp. 104-111.